# Investigation of core machinery for biosynthesis of Vi antigen capsular polysaccharides in Gram-negative bacteria

Received for publication, October 25, 2021, and in revised form, December 1, 2021 Published, Papers in Press, December 9, 2021,
https://doi.org/10.1016/j.jbc.2021.101486

**Samantha S. Wear[1], Caitlin Sande[1], Olga G. Ovchinnikova[1], Andrew Preston[2], and Chris Whitfield[1,*]**

*From the [1]Department of Molecular and Cellular Biology, University of Guelph, Guelph, Ontario, Canada; [2]Milner Centre for Evolution and Department of Biology and Biochemistry, University of Bath, Claverton Down, Bath, UK*

Edited by Gerald Hart

***Salmonella enterica*** **serovar Typhi causes typhoid fever. It possesses a Vi antigen capsular polysaccharide coat that is important for virulence and is the basis of a current glycoconjugate vaccine. Vi antigen is also produced by environmental *Bordetella* isolates, while mammal-adapted *Bordetella* species (such as *Bordetella bronchiseptica*) produce a capsule of undetermined structure that cross-reacts with antibodies recognizing Vi antigen. The Vi antigen backbone is composed of poly-α-(1→4)-linked *N*-acetylgalactosaminuronic acid, modified with *O*-acetyl residues that are necessary for vaccine efficacy. Despite its biological and biotechnological importance, some central aspects of Vi antigen production are poorly understood. Here we demonstrate that TviE and TviD, two proteins encoded in the *viaB* (Vi antigen production) locus, interact and are the Vi antigen polymerase and *O*-acetyltransferase, respectively. Structural modeling and site-directed mutagenesis reveal that TviE is a GT4-family glycosyltransferase. While TviD has no identifiable homologs beyond Vi antigen systems in other bacteria, structural modeling suggests that it belongs to the large SGNH hydrolase family, which contains other *O*-acetyltransferases. Although TviD possesses an atypical catalytic triad, its *O*-acetyltransferase function was verified by antibody reactivity and $^{13}$C NMR data for *tviD*-mutant polysaccharide. The *B. bronchiseptica* genetic locus predicts a mode of synthesis distinct from classical *S. enterica* Vi antigen production, but which still involves TviD and TviE homologs that are both active in a reconstituted *S.* Typhi system. These findings provide new insight into Vi antigen production and foundational information for the glycoengineering of Vi antigen production in heterologous bacteria.**

Many bacteria are surrounded by a hydrated capsule layer composed of high-molecular-weight capsular polysaccharide (CPS) (1). In many pathogens, capsules are crucial virulence determinants; they can maintain a hydrated surface layer, aid in biofilm formation, and protect against complement-mediated killing and opsonophagocytosis (1–3). CPS structures are highly variable in their sugar composition, linkages, and nonsugar modifications. Despite this diversity, the assembly of capsular layers in Gram-negative bacteria is predominantly accomplished *via* one of two strategies (1).

In one assembly strategy, CPS molecules are synthesized at the cytoplasm–cytoplasmic membrane interface and are then exported to the cell surface using a dedicated trans-envelope system. The export machinery consists of an ATP-binding cassette (ABC) transporter, a (predominantly) periplasmic protein belonging to polysaccharide copolymerase family 3 (PCP-3), and an outer membrane polysaccharide export (OPX) translocon. *Escherichia coli* "group 2" capsules provide the prototype for this pathway (1). Sequence data (sometimes supported by mutant phenotypes) suggest that this translocation strategy is shared by several human pathogens, including extraintestinal pathogenic *E. coli*, *Salmonella enterica* serovar Typhi, *Bordetella pertussis*, *Haemophilus influenzae*, *Campylobacter jejuni*, and *Neisseria meningitidis*. Most of these bacteria are believed to generate CPS with a characteristic glycolipid at the reducing terminus, based on possession of genes encoding two CMP-3-deoxy-D-*manno*-oct-2-ulosonic acid (CMP-Kdo)-dependent glycosyltransferases (GTs), KpsS and KpsC. The functions of KpsS and KpsC have been characterized biochemically and structurally in *E. coli* (4–7). They build a short β-Kdo oligosaccharide on phosphatidylglycerol acceptor, and this molecule serves as a shared acceptor for CPS structure-specific GTs to polymerize repeat unit polymers by growth at the nonreducing terminus (5, 6, 8). The terminal glycolipid is thought to provide a signal recognized by the export machinery to facilitate translocation of the completed product to the cell surface (1).

Currently, one variation of this prototype is known. This is the Vi antigen CPS produced by typhoidal isolates of *S. enterica* serovar Typhi, *Citrobacter freundii*, and some members of the *Burkholderiales* such as the soil bacteria *Bordetella petrii* and members of the genera *Achromobacter* and *Orrella* (9–12). These bacteria possess homologs of the standard export-translocation machinery but are unable to synthesize the phosphatidyl-β-Kdo oligosaccharide acceptor due to the lack of the *kpsSC* genes. Although the structure and function of Vi antigen have not been studied in soil *Burkholderiales*, its properties and importance in the ability of *S.* Typhi to cause typhoid fever are well established. *S.* Typhi Vi antigen CPS is composed of a linear polymer of α-(1→4)-linked *N*-acetylgalactosaminuronic acid (GalNAcA) that is

* For correspondence: Chris Whitfield, cwhitfie@uoguelph.ca.

nonstoichiometrically *O*-acetylated at C-3 (13, 14). Vi antigen production differentiates *S.* Typhi from nontyphoidal *Salmonellae* that cause gastroenteritis. The importance of Vi antigen in pathogenicity was demonstrated in a murine model of infection, where the $LD_{50}$ increased approximately 10,000-fold for *S.* Typhi variants lacking Vi antigen (15, 16). Vi antigen participates in the evasion of the host immune system by reducing deposition of complement component 3b on the bacterial surface and clearance of *S.* Typhi by macrophages (17, 18). Purified Vi antigen is currently used in some vaccine formulations for typhoid fever, with the *O*-acetyl groups being essential for protection (19–21).

The ten-gene *viaB* locus in *S.* Typhi encodes proteins required for transcriptional regulation of Vi production and biosynthesis (*tvi* genes) and translocation (*vex* genes) (9, 22, 23) (Fig. 1, *A* and *B*). The minimal set of genes required to produce Vi antigen is *tviBCDE*; transposon insertions in any of these genes are known to abolish Vi antigen production (22, 23). Production of the Vi-cytoplasmic sugar nucleotide precursor, UDP-GalNAcA, is catalyzed by TviBC (24) (Fig. 1*B*). Vi antigen possesses a diacyl-HexNAc reducing terminus whose structure has not been definitively resolved. VexE is a dedicated acyltransferase associated with proper acylation and is essential for efficient export and for retention of the CPS glycan at the cell surface (9). However, the enzymes responsible for Vi-polymerization and acetylation have not been clearly established. Resolving their functions is central to the long-term goal of unravelling the full assembly-export

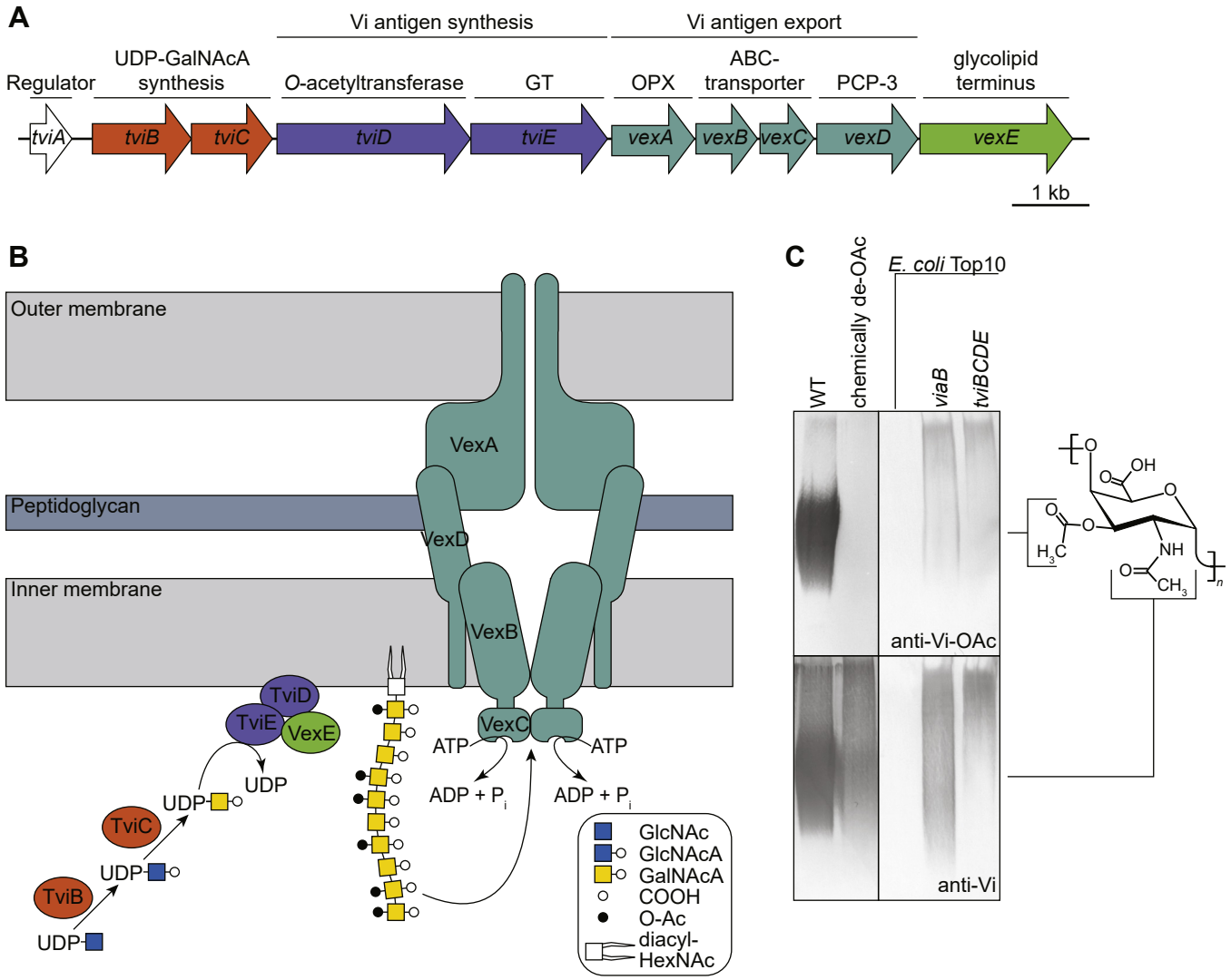


**Figure 1. Vi antigen biosynthesis.** *A,* genetic organization of the *viaB* locus from *S.* Typhi. *B,* model of Vi antigen assembly and export. In the cytoplasm, TviBC synthesizes UDP-GalNAcA, the nucleotide sugar precursor. The UDP-GlcNAc C-6 dehydrogenase (TviB) oxidizes UDP-GlcNAc to UDP-GlcNAcA, and this is converted to UDP-GalNAcA by the UDP-GlcNAcA epimerase (TviC). TviDE is hypothesized to be required for polymerization and *O*-acetylation, while VexE is a dedicated acyltransferase that modifies a HexNAc residue at the reducing terminus; the enzymatic origin of the HexNAc and details of the terminal structure are currently unknown. Once completed, the Vi polysaccharide is exported by an ABC transporter (VexBC), a polysaccharide copolymerase family-3 protein (VexD), and an outer membrane export protein (VexA). VexE-mediated modification is essential for Vi retention at the cell surface. *C,* Western immunoblots demonstrating differential reactivities of anti-Vi-OAc monoclonal antibody and anti-Vi polyclonal antibody, which recognizes the glycan backbone independent of *O*-acetyl groups. The samples are purified WT Vi and chemically de-*O*-acetylated Vi (*left*) as reactivity controls and proteinase K-digested whole-cell lysates of *E. coli* Top10 transformants harboring the entire *viaB* cluster or *tviBCDE* showing products made in recombinant strains with and without Vi export, respectively (*right*). The immunoblot is representative of three biological replicates.

pathway for an influential CPS-assembly prototype and may enable new strategies for vaccine production by *in vivo* glycoengineering or by *in vitro* chemi-enzymatic methods. Here, we demonstrate that TviE is the sole GT required (and sufficient) for polymerization and TviD is the Vi antigen *O*-acetyltransferase.

## Results

### *TviBCDE is sufficient for biosynthesis of O-acetylated Vi antigen in an* E. coli *host*

TviBCDE is sufficient for production of intracellular Vi antigen in recombinant *E. coli* (22, 23), but the *O*-acetylation status of this product from these proteins was not investigated. This was examined using differential antibody reactivities. Two antigenic determinants have been described for Vi antigen: the *O*-acetyl present at C-3 and the *N*-acetyl and carboxyl moieties associated with the glycan backbone (21, 25). Monoclonal antibody P2B1G2/A9 recognizes an epitope dependent on the *O*-acetyl groups (25), and its reported specificity was confirmed by the loss of reactivity in Western immunoblots of purified Vi antigen, following chemical de-*O*-acetylation (Fig. 1*C*). Here, this antibody is designated "anti-Vi-OAc." In contrast, the reactivity of a rabbit polyclonal antibody ("anti-Vi") was unaffected by the removal of *O*-acetyl groups. In Western blots of proteinase K-digested whole-cell lysates, both antibodies react with a disperse range of Vi antigen chain lengths produced by *E. coli* Top10 harboring plasmids containing either the complete *viaB* locus (plasmid pWQ783) or *tviBCDE* alone (pWQ1045) (Fig. 1*C*). As expected, *E. coli* Top10 cells transformed with plasmid containing *viaB* produced a capsular layer reactive with both antibodies, which was revealed by immunofluorescence microscopy of fixed cells (Fig. S1). In contrast, *E. coli* Top10 cells containing *tviBCDE* accumulated Vi antigen in intracellular inclusion bodies, which have been previously reported in mutants with compromised export (9). Reactivity with both antibodies was retained, ruling out the possible involvement of periplasmic *O*-acetylation known in some glycoconjugate-assembly systems (26) (Fig. S1). These data establish that the necessary GT and *O*-acetyltransferase activities for Vi antigen production are encoded within the *tviBCDE* gene block and stimulated further investigation of TviD and TviE.

### *TviE is a UDP-GalNAcA-dependent glycosyltransferase*

TviE is the only identifiable GT encoded by the *viaB* locus and, while similarity shared between TviE and GTs has been reported (22), the details have not been investigated. The C-terminus of TviE contains a putative GT domain belonging to the GT4 family in the CAZy database (27) and is annotated as such by the Conserved Domain Database (CDD) (28) (Fig. 2*A*). Well-studied examples of GT4 enzymes include: WaaG from *E. coli* (29), PimA from *Mycobacterium smegmatis* (30), WbdA from *E. coli* (31), and PglH from *C. jejuni* (32). These representatives possess a GT-B fold, act *via* a retaining glycosylation mechanism, and utilize nucleoside diphosphate (NDP)-activated sugars as donor substrates (33). To provide further insight into the putative TviE GT4 domain, and the organization of the enzyme, the sequence of TviE was submitted to Phyre2 (34). The top five models were all created using members of the GT4 family as templates. These templates (in ranked order) are: sucrose synthase-1 from *Arabidopsis thaliana* (AtSus1: PDB 3S29), sucrose synthase from *Nitrosomonas europaea* (Ss2: PDB 4RBN), sucrose phosphate synthase from *Halothermothrix orenii* (SpsA: PDB 2R60), D-inositol-3-phosphate GT from *Corynebacterium glutamicum* (MshA: PDB 3C4V), and α-mannosyltransferase from *C. glutamicum* (PimB: 3OKA). The sequences of the C-terminal GT4 modules align well (Fig. S2), and Phyre2 (34) predicts with 100% confidence that TviE and each of the templates are homologous. In addition to the identifiable GT4 modules, AtSus1, Ss2, and TviE all possess additional N-terminal sequences that vary in size and share little similarity.

The highest ranked model for TviE is based on the structure of AtSus1, where the GT4 modules (TviE, residues 163–562; AtSus1, residues 277–776) share only 25% identity (Fig. S3). Despite the low primary sequence homology, the entire sequence of TviE was modeled and predicts a GT domain located between residues 163–562. This region of the structure predicts two Rossmann folds, which is characteristic of GT-B-fold enzymes, like those of the GT4 family (27) (Fig. 2*B*). GT4 enzymes possess active site $EX_7E$ motifs, which are involved in binding nucleotide sugar donors (Fig. 2, *B* and *C*). In biochemically characterized representatives, the first Glu residue of the $EX_7E$ motif interacts with the sugar moiety of the NDP-sugar donor, while the 2′ and 3′ hydroxyl groups of the ribose sugar form hydrogen bonds with the second Glu (30, 32, 35). The relative importance of either of the Glu residues varies in different GT4 enzymes (30, 36–39). In some, both residues are essential for activity but, in others, one residue is expendable. The functional importance of these residues was investigated in TviE.

Vi antigen was expressed in *E. coli* BL21(DE3) from a plasmid containing the *viaB* locus (pWQ783) and reacted with both anti-Vi-OAc and anti-Vi antibodies (Fig. 2*D*). Deletion of *tviE* from plasmid-encoded *viaB* (*viaB*-Δ*tviE*; pWQ1042) eliminated reactivity of the corresponding proteinase K-digested whole-cell lysate with either antibody (Fig. 2*D*), consistent with the previously described phenotype of a *tviE* transposon-insertion mutant (22, 23). Overexpression of $His_6$-TviE restored Vi antigen production in *E. coli* BL21(DE3) expressing *viaB*-Δ*tviE*. To evaluate the importance of the $EX_7E$ motif for the activity of TviE, $His_6$-$TviE^{E483A}$ and $His_6$-$TviE^{E491A}$ mutants were made. Neither was able to support Vi antigen synthesis, indicating both Glu residues of the $EX_7E$ motif are essential in TviE (Fig. 2*D*). Whole-cell lysates were probed with anti-$His_5$ antibody to verify both mutant proteins were expressed (Fig. 2*D*) and subcellular localization determined that the majority of each protein localized to the soluble fraction (S100; 100,000*g*) (Fig. S4*A*). Furthermore, the melting temperatures of the mutant proteins in thermal shift assays fell

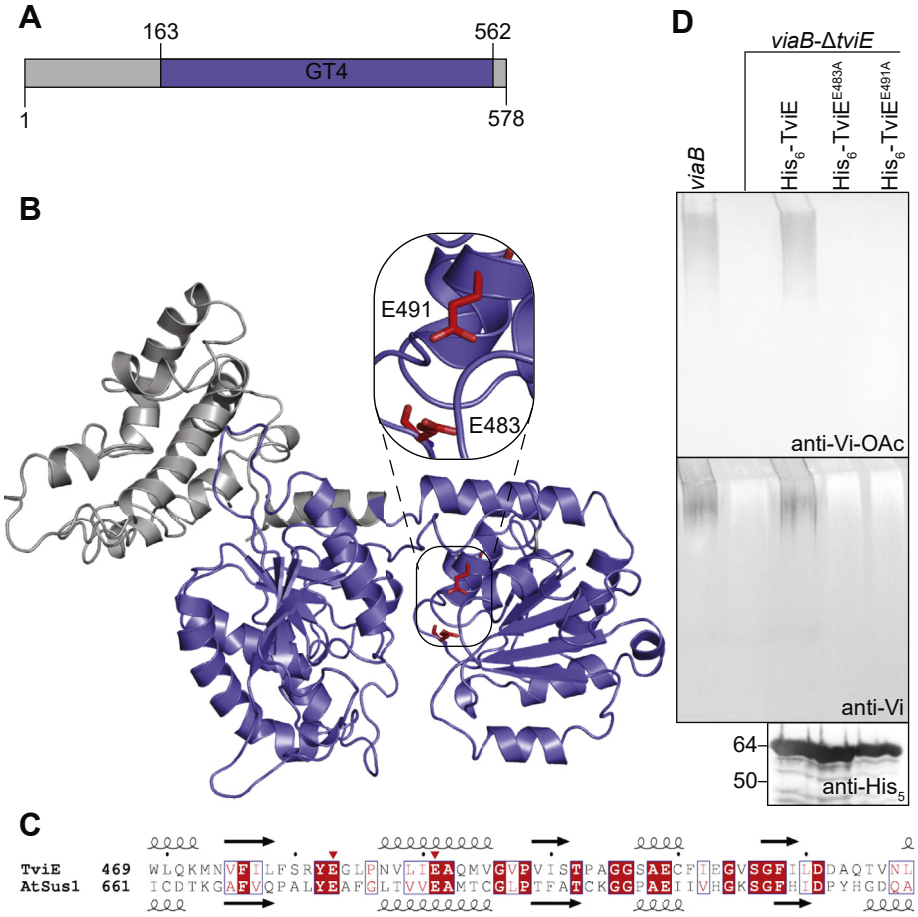


**Figure 2. Activity and predicted structure of TviE.** *A,* predicted domain organization of TviE from the CDD (28). *B,* TviE structural model generated by Phyre2 (34) using sucrose synthase-1 from *A. thaliana* (AtSus1: PDB 3S29) as a template. The active site with the $EX_7E$ motif is highlighted with the Glu residues depicted as *red sticks*. *C,* sequence and secondary structure alignment of the $EX_7E$-containing region of TviE and AtSus1. The predicted secondary structure of TviE and the solved structure of AtSus1 are displayed *above* and *below* the alignment, respectively. Predicted α-helices and β-strands are depicted by *helices* and *arrows*, respectively. Proposed catalytic Glu residues of the $EX_7E$ motif are indicated with a *red triangle*. The alignment was generated with ClustalW (73) and displayed using ESPript (74). A complete alignment is shown in Fig S3. *D,* Western immunoblots of proteinase K-digested whole-cell lysates from *E. coli* BL21(DE3) recombinants showing the absence of Vi antigen production in constructs with *tviE* deleted. The mutation is complemented using plasmids expressing *tviE in trans*, and activity is eliminated by mutating Glu residues in the $EX_7E$ motif. Expression of TviE and its mutants was confirmed by probing protein lysates with anti-$His_5$ antibody. The control (*viaB*) is *E. coli* BL21(DE3) transformed with plasmid pWQ783 containing the complete *viaB* locus. All other samples were from *E. coli* BL21(DE3) transformants. Western immunoblots are representative of three biological replicates.

within 2 °C of wild-type $His_6$-TviE (Fig. S4*B*), ruling out global changes in stability as an explanation for loss of activity of the mutant protein.

The N-terminal 276 residues of AtSus1 form a predominantly α-helical structural element required for cellular targeting. This region also binds plant host-derived peptides, which are involved in root nodule formation in legumes. This part of the structure is positioned away from the GT4 domain (35). Residues 1–36 of TviE align with residues 118–167 of AtSus1, which correspond to the end of the cellular targeting domain region (residues 11–127) and the first part of the peptide-binding region (residues 157–276) (Fig. S3) and could only be modeled with low confidence. The remaining sequence of TviE preceding the GT4 module (residues 37–162) was modeled with high confidence and is therefore predicted to be predominantly α-helical, like AtSus1 (35) (Figs. 2*B* and S3). Since the N-terminal part of TviE possesses no informative motifs, its functional importance in Vi antigen synthesis was investigated by removing residues 1–162. Removal of the entire N-terminal domain ($His_6$-$TviE^{163–578}$) rendered the protein inactive based on its inability to complement *viaB*-Δ*tviE* defect in *E. coli* BL21(DE3) and restore antibody reactivity in proteinase K-digested whole-cell lysates (Fig. S5*C*). However, cellular fractionation showed that the $His_6$-$TviE^{163–578}$ protein was predominantly found as inclusion bodies and within cellular debris (P12; 12,000*g*), with a small amount associated with the membrane fraction (P100; 100,000*g*) (Fig. S5*D*). A longer truncation mutant ($His_6$-$TviE^{50–578}$) removing only two short α-helices, with the endpoint located in a loop, was made in an attempt to minimally disrupt secondary structure elements. $His_6$-$TviE^{50–578}$ was present in the soluble fraction (S100) and the thermal shift profile did not deviate from the wild-type protein (Fig. S5, *D* and *E*). However, $His_6$-$TviE^{50–578}$ was unable

to restore Vi antigen synthesis (Fig. S5*C*), suggesting that the N-terminal α-helical structure is essential for function in Vi antigen synthesis.

### *TviD is a novel O-acetyltransferase*

Functions have been assigned to all of the *viaB* genes, except for *tviD*, making *tviD* a candidate for the gene encoding the missing Vi antigen *O*-acetyltransferase. A transposon insertion in *tviD* abolishes Vi antigen production in *E. coli* harboring the mutated *viaB* locus (23); however, detection of Vi antigen in this previous study relied solely on the anti-Vi-OAc antibody. Thus, it was unclear whether the phenotype reflected loss of polymer production or loss of the *O*-acetyl epitope. To distinguish these possibilities, the *tviD* gene was deleted from the *tviABCDE*-containing plasmid (creating pWQ1046; *tviABCE*). Proteinase K-digested whole-cell lysates from *E. coli* Top10 cells harboring *tviABCE* showed a reactivity profile (Fig. 3*A*) resembling chemically de-*O*-acetylated Vi antigen (Fig. 1*C*). These data are consistent with a model in which TviD is the *O*-acetyltransferase, and its activity is not required for polymerization of the Vi antigen backbone. Overexpression

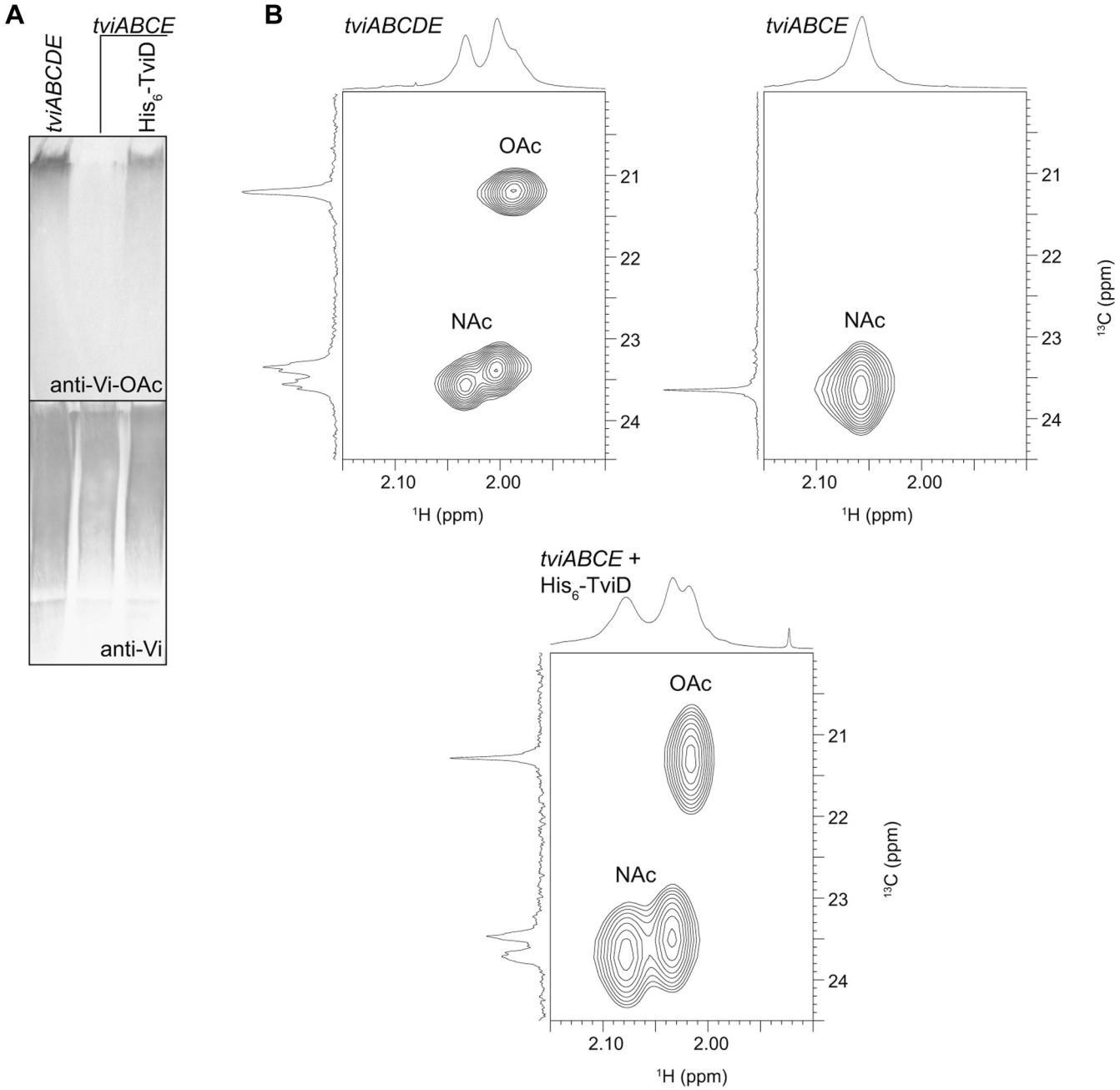


**Figure 3. TviD is required for Vi antigen *O*-acetylation.** *A,* Western immunoblots of proteinase K-digested lysates from *E. coli* Top10 harboring a plasmid encoding TviABCDE produces intracellular (see Fig. S1 - TviBCDE) Vi antigen reacting with both antibodies. Deletion of *tviD* (TviABCE) eliminates reactivity with the anti-Vi-OAc monoclonal antibody only, and this is restored by introducing a plasmid expressing $His_6$-TviD *in trans*. Western immunoblots are representative of three biological replicates. *B,* Parts of $^{1}H,^{13}C$ HSQC spectra of purified Vi antigen from the samples shown in panel *A*, demonstrating correlations of methyl groups of *N*- and *O*-acetyl groups.

of $His_6$-TviD (pWQ1052) restored production of *O*-acetylated Vi antigen in *E. coli* Top10 containing *tviABCE*, thus attributing the Vi antigen phenotype solely to the *tviD* mutation (Fig. 3*A*).

To definitively confirm that the absence of *tviD* only affected *O*-acetyl content, Vi antigen was purified from *E. coli* Top10 cells expressing TviABCDE, TviABCE, and TviABCE [$His_6$-TviD]. The $^{13}C$ NMR spectra of Vi antigens from cells expressing TviABCDE and TviABCE[$His_6$-TviD] were comparable to published data (9) (Fig. 3*B*). In contrast, the $^{13}C$ NMR spectrum from cells expressing only TviABCE lacked the diagnostic peak (21.2 ppm) corresponding to *O*-acetyl groups (Fig. 3*B*), like chemically de-*O*-acetylated Vi antigen (9). This data provided the foundation to further explore the activity of TviD.

TviD is separated into two domains. The N-terminal part of the protein (~320 residues) has no identifiable homologs of known function in BLAST (40) searches (other than TviD proteins encoded by other *viaB* loci), nor does it contain any informative motifs. In contrast, the C-terminal part of the protein contains two distinct putative tetratricopeptide repeat (TPR) regions with four and five repeats, respectively (Fig. 4*A*). These repeats were predicted with 99.6% probability by TPRpred (41, 42). The TPR-containing region comprises over 60% of TviD and complicates modeling of the N-terminal domain, which was presumed to form the *O*-acetyltransferase. To produce a model offering insight into the putative catalytic domain, the TPR region of the protein was excluded. The N-terminal sequence (residues 1–322) was submitted to RaptorX (43), and the highest-scoring models were created using members of the SGNH hydrolase family from *Enterococcus faecalis* (PDB 1YZF), *Veillonella parvula* (PDB 4RW0), a predicted protein from the metagenome of Lake Arreo, Spain (PDB 5JD3), *Alicyclobacillus acidocaldarius* (PDB 3RJT), and *Geobacillus stearothermophilus* (Axe2: PDB 3W7V) (Fig. S6). None of the templates are known *O*-acetyltransferases, but the SGNH hydrolase family is comprised of a large group of esterases, lipases, and transferases and does include some established *O*-acetyltransferases (44–46). As the name suggests, SGNH proteins typically possess a conserved Ser, Gly, Asn, and His in their active sites (44).

The top-ranked model was produced using the uncharacterized acyl hydrolase/lipase from *E. faecalis* (PDB 1YZF) as the template (Fig. 4*B*). The model has a *p* value of $5.15e^{-3}$,

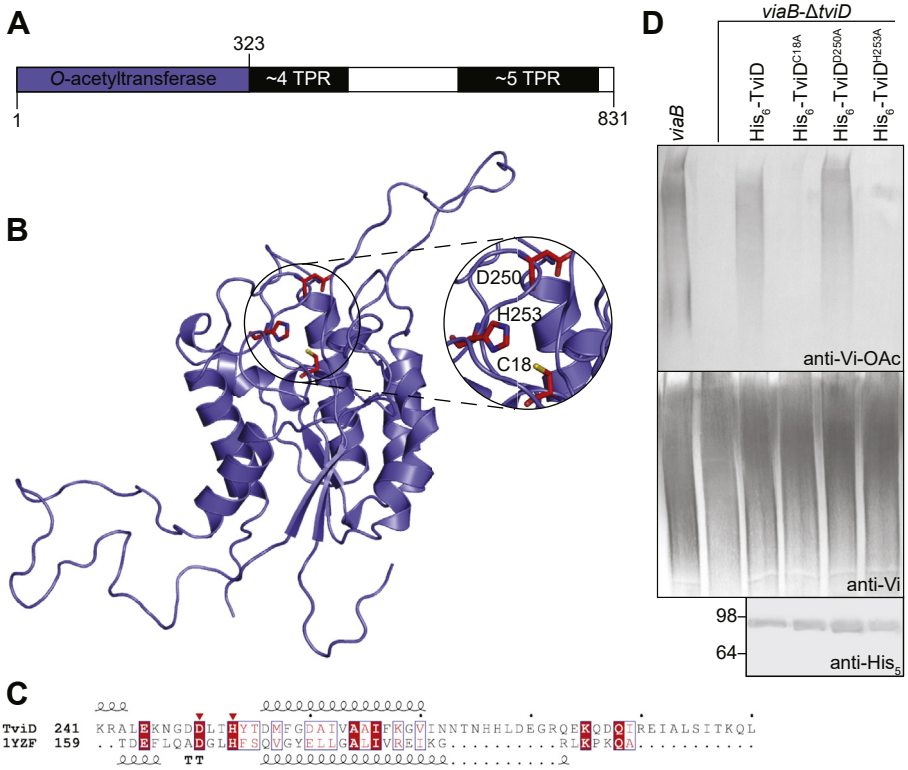


**Figure 4. Activity and predicted structure of TviD.** *A,* Predicted domain organization of TviD with putative C-terminal TPR domain based on TPRpred (41, 42). *B,* Structural model of the N-terminal part of TviD (residues 1–322). The model was generated by RaptorX (43) using an uncharacterized acyl hydrolase/lipase from *E. faecalis* (PDB 1YZF) as a template. Residues 277–322 form an extended loop and were removed here to highlight the putative active site (*inset*). Candidate catalytic residues are depicted as *red sticks*. *C,* sequence and secondary structure alignment of the DXXH motif-containing region of $TviD^{1–322}$ and 1YZF. The predicted secondary structure of $TviD^{1–322}$ and the solved structure of 1YZF are displayed *above* and *below* the alignment, respectively. Alpha-helices and strict β-turns are represented by helices and TT, respectively. The conserved Asp and His of the DXXH motif are indicated with a *red triangle*. The alignment was generated with ClustalW (73) and displayed with ESPript (74). Alignment of the complete proteins is shown in Fig. S7. *D,* Western immunoblots of proteinase K-digested whole-cell lysates from *E. coli* Top10 recombinants showing the absence of *O*-acetylation of Vi antigen in constructs with *tviD* deleted. The mutation is complemented using plasmids expressing *tviD in trans*, and activity is eliminated by mutating Cys18 or His253. Expression of TviD and its mutants was confirmed by probing protein lysates with anti-$His_5$ antibody. The control (*viaB*) and other constructs were transformed into *E. coli* Top10. Western immunoblots are representative of three biological replicates.

indicating a model of good quality, despite limited sequence identity (~18%) shared between 1YZF and TviD$^{1-322}$ (Fig. S7). 1YZF possesses a canonical α/β hydrolase fold, conserved among members of the SGNH hydrolase family, and this is predicted in the TviD$^{1-322}$ model (Fig. 4*B*). Residues 277–322 form a long loop, which extends away from the rest of the structure and does not align well with the sequence of 1YZF (Fig. S7), so these residues were excluded in the model to focus on the putative active site (Fig. 4*B*). SGNH hydrolases typically possess four consensus sequence blocks with the conserved Ser-His-Asp catalytic triad housed in blocks I and V (44, 47). Block I contains the nucleophilic Ser in the GDS motif. Based on the alignment results (Fig. S6), TviD does not possess a typical block I and instead has a conserved Gly followed by Ser-Cys, which creates a gap in the alignment. The residue representing the nucleophile is not apparent from the sequence alignment alone, but Ser17 and Cys18 are both candidates based on proximity in the model. Although Cys is an atypical nucleophile, Cys18 has the correct orientation in the model to act as a nucleophile; it extends into the active site and is found on a loop adjacent to Asp250 and His253 (Fig. 4*B*). Sequence alignments suggest that Asp250 and His253 make up the conserved DXXH motif (block V) (Figs. 4*C* and S6).

To investigate the role of these putative catalytic residues in His$_6$-TviD, site-directed mutagenesis was used to convert each residue to Ala, and the mutant variants were tested for their ability to restore *O*-acetylation in *E. coli* Top10 transformed with *viaB*-Δ*tviD* (pWQ1041). His$_6$-TviD$^{C18A}$ and His$_6$-TviD$^{H253A}$ were unable to restore *O*-acetylation based on reactivity with the anti-Vi-OAc antibody (Fig. 4*D*). In contrast, His$_6$-TviD$^{D250A}$ restored activity to the *viaB*-Δ*tviD* mutant (Fig. 4*D*). The alternative nucleophile candidate, Ser17, also proved to be unimportant for activity (data not shown). To verify that the lack of *O*-acetyltransferase activity was not due to altered protein expression, lysates were probed in Western immunoblots with anti-His$_5$ antibody (Fig. 4*D*). In further analysis, the majority of His$_6$-TviD and mutant variants localized to the membrane (P100) (Figs. 5*B* and S8*A*). Checking protein folding for the full-length protein was compromised by its membrane association so, instead, folding was assessed using soluble truncated forms containing only residues 1–322, encompassing the functional catalytic domain (see below). Protein thermal melt curves confirmed that all of the truncated variants possessed similar melting temperatures (Fig. S8*B*). Based on these results, we propose that TviD catalysis is dependent on either an atypical Cys-His-Asp triad or a Cys-His dyad.

### *The TPR domain of TviD is not essential for O-acetyltransferase activity*

The C-terminal TPR domain of TviD contains nine putative TPR motifs; four located between residues 323 and 461 and five between residues 614 and 809 (Fig. 5*A*). To investigate the role of each TPR region, three sequential C-terminal truncations were made, beginning by removing the five TPRs (His$_6$-TviD$^{1-613}$) and then extending to include the intervening region between the two sets of TPRs (His$_6$-TviD$^{1-461}$) and finally the entire TPR region (His$_6$-TviD$^{1-322}$). To avoid disruption of α-helices, the end points for these truncations were located between predicted secondary structure elements. Cellular fractionation and Western immunoblots with anti-His$_5$ antibody revealed that His$_6$-TviD$^{1-613}$ localized to the membrane fraction (P100) like His$_6$-TviD (Fig. 5*B*). Two putative membrane-associated amphipathic helices were predicted at the C-terminus (residues 528–545 and 731–748) by HELIQUEST (48). In contrast, the majority of His$_6$-TviD$^{1-461}$ and His$_6$-TviD$^{1-322}$ were in the soluble fraction (S100) (Fig. 5*B*). These data implicate the C-terminus of TviD (residues 614–831) as being essential for membrane association.

To determine whether the truncated proteins retain *O*-acetyltransferase activity, *E. coli* Top10 was transformed with a plasmid carrying *viaB*-Δ*tviD* and another encoding either His$_6$-TviD$^{1-322}$, His$_6$-TviD$^{1-461}$, or His$_6$-TviD$^{1-613}$. Each of the truncation derivatives restored Vi antigen *O*-acetylation (Fig. 5*C*). Therefore, the TPRs are not essential for *O*-acetylation under these (plasmid expression) conditions. Immunofluorescence was performed to verify that the Vi antigen made in the presence of truncated TviD was still retained at the cell surface, to rule out the possibility of any unanticipated effects of the deletions on polymer export. As expected, *viaB*-Δ*tviD* cells only reacted with the anti-Vi antibody (Fig. 5*D*). Overexpression of His$_6$-TviD or His$_6$-TviD$^{1-322}$ restored surface assembly of *O*-acetylated Vi antigen, which reacted with both Vi antigen antibodies (Fig. 5*D*). These results established that the *O*-acetyltransferase catalytic domain resides between residues 1 and 322 and that the TPR structure is not essential for polymer biosynthesis, *O*-acetylation, or polysaccharide export under these conditions.

### *TviD and TviE interact via the TPR domain of TviD*

TPR domains frequently mediate protein–protein interactions within complexes (49). TviE has an N-terminal domain of unknown function, leading to the hypothesis that these noncatalytic elements might participate in interactions between these proteins. To pursue this, a plasmid (pWQ1059) was created to coexpress His$_6$-TviD and TviE-FLAG. This construct maintains the native arrangement of the genes, which overlap by one nucleotide (Fig. 6*A*). Since TviD is membrane-associated, membranes from *E. coli* Top10 [pWQ1059] were collected and solubilized with lauryldimethylamine oxide (LDAO). The solubilized protein fraction was isolated, and potential His$_6$-TviD/TviE-FLAG interactions were probed using a copurification strategy involving Ni-NTA chromatography. Western immunoblots using epitope-specific antibodies were used to detect His$_6$-TviD and TviE-FLAG (Fig. 6*B*). The analysis was complicated by the proteins becoming substantially more susceptible to proteolytic degradation after detergent solubilization (compare to Figs. S4*A* and 5*B* for samples without detergent solubilization), but interaction data were obtained. The expected molecular mass of His$_6$-TviD is 96.8 kDa and the anti-His$_5$

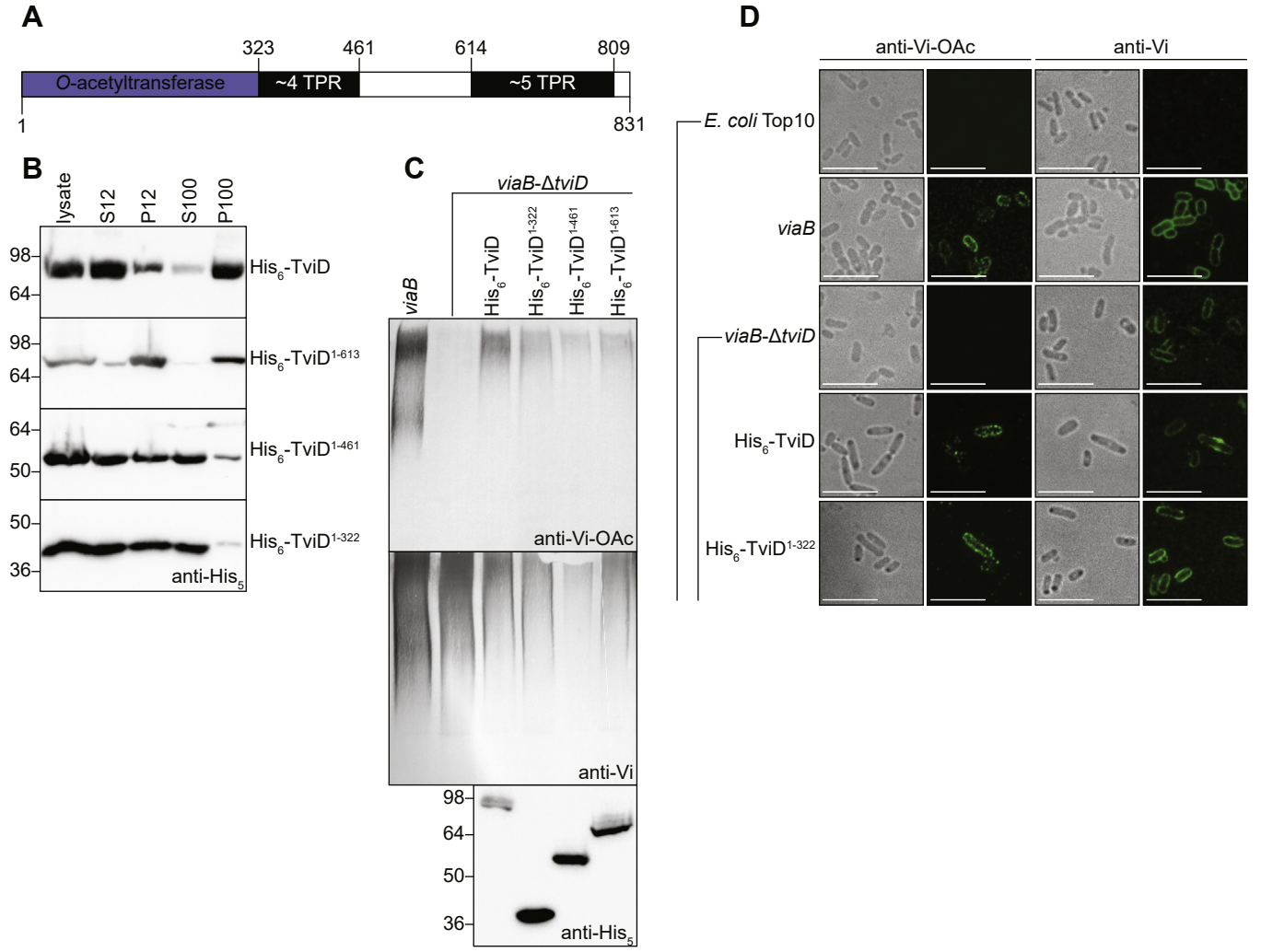


**Figure 5. Importance of the TPR-containing domain of TviD for subcellular localization.** *A,* Predicted domain organization with TPR regions predicted by TPRpred (41, 42). *B,* Cellular distribution of TviD and C-terminal deletion constructs expressed in *E. coli* Top10. Protein was detected by Western immunoblots probed with anti-$His_5$ antibody. S12 and P12 are soluble and pelleted fractions, respectively, from centrifugation at 12,000*g*, while S100 and P100 are the corresponding fractions obtained after centrifugation of the S12 fraction at 100,000*g*. The pH of the resuspension buffer used for the analysis of all proteins was 7.4. *C,* Western immunoblots of proteinase K-digested whole-cell lysates from *E. coli* Top10 recombinants showing that *O*-acetylated Vi antigen is produced by expression of TviD, or its C-terminally-truncated derivatives, *in trans* to complement the *tviD* deletion. Expression of TviD and the truncation mutants was confirmed by probing protein lysates with anti-$His_5$ antibody. The control (*viaB*) and other constructs were transformed into *E. coli* Top10. *D,* Immunofluorescence microscopy of *E. coli* Top10 (negative control) and a transformant containing a plasmid carrying the *viaB* locus (positive control). $His_6$-TviD and $His_6$-$TviD^{1-322}$ were expressed in the *tviD*-deletion. Cells were probed with anti-Vi-OAc and anti-Vi antigen primary antibodies and fluorescent secondary antibodies for Vi antigen detection. All transformants produced surface-expressed Vi antigen. Scale bars represent 7 μm. All experiments are representative of three biological replicates.

detects two prominent Ni-NTA-bound proteins (eluted with imidazole) with apparent sizes of 93.1 kDa and 80.0 kDa, indicating some proteolytic cleavage in the C-terminal region. TviE-FLAG has a calculated size of 66.0 kDa, and the anti-FLAG antibody reveals an apparently intact protein (apparent size 65.7 kDa), together with a smaller C-terminal fragment (48 kDa). Although TviE is predominantly soluble when expressed alone (Fig. S4*A*), a portion of the protein and its degradation product was retained by Ni-NTA in the presence of membrane-associated $His_6$-TviD (Fig. 6*B*). When the two proteins were subjected to Ni-NTA chromatography in the absence of their partner, $His_6$-TviD (and its fragment) bound to the resin, while TviE-FLAG (and its fragment) eluted in the unbound fraction, as expected (Fig. S9, *A* and *B*), ruling out nonspecific interactions of TviE-FLAG with the resin. These results support protein–protein interactions and a complex containing TviD and TviE (Fig. 6*B*).

To examine the potential role of the TPR domain of TviD in interactions, the codons for residues Pro323 and Val324 were each replaced with stop codons to truncate TviD before the C-terminal TPR domain (Fig. 6*A*). In the absence of the TPR domain, $His_6$-$TviD^{1-322}$ is soluble (Fig. 5*B*) (like $His_6$-TviE; Fig. S4*A*), therefore, the Ni-NTA copurification strategy was performed using the S100 fraction. Under these conditions, $His_6$-$TviD^{1-322}$ (expected molecular mass of 38.4 kDa) has minimal degradation, since the C-terminal proteolytically susceptible domain is absent. Most of the protein was bound to the Ni-NTA resin and subsequently eluted with imidazole

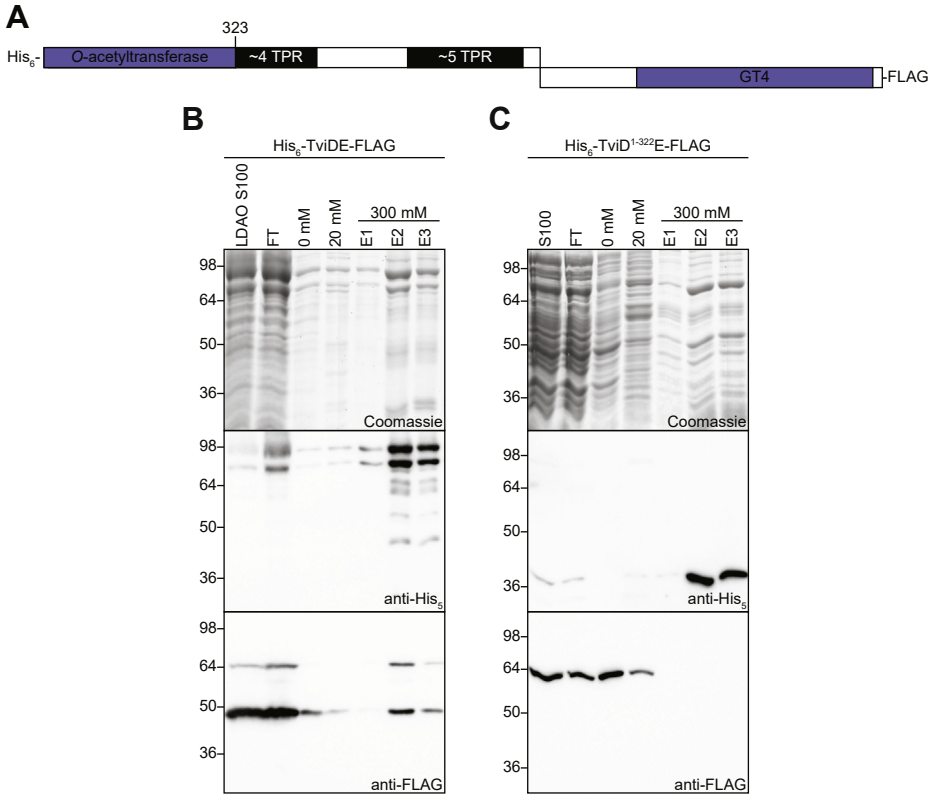


**Figure 6. TviD and TviE interact.** *A,* Organization of the expression construct used for analyzing $His_6$-TviD/TviE-FLAG interactions, which was expressed in *E. coli* Top10. *B,* LDAO was used to solubilize TviD from the membrane fraction, and the detergent extract was loaded onto an Ni-NTA column. The unbound flow-through (FT), imidazole washes (0 mM and 20 mM), and elution fractions (E1–3) are shown. Samples from each fraction were separated by SDS-PAGE, and proteins were visualized using Coomassie stain and Western immunoblotting with anti-$His_5$ and anti-FLAG antibodies. The elution fractions contained both $His_6$-TviD and TviE-FLAG. *C,* Replication of the experiment with a plasmid expressing $His_6$-$TviD^{1-322}$E-FLAG eliminated the interaction. The resuspension buffer used for both experiments had a pH of 7.4 and the washes contained 0 and 20 mM imidazole. Copurification results are representative of three biological replicates.

(Fig. 6*C*). In the absence of LDAO, TviE-FLAG does not undergo N-terminal degradation but is no longer retained on the Ni-NTA resin. These data indicate that the TPR domain of TviD is required for its ability to interact with TviE.

### Bordetella *species possess TviDE homologs and produce a CPS related to Vi antigen*

Loci resembling *viaB* from *S.* Typhi are found in soil-inhabiting species of members of the Burkholderiaceae (including some *Bordetell*a species) and the VexE protein from *A. denitrificans* can replace the *S.* Typhi homolog (9). In contrast, human and animal adapted *Bordetella* sp., such as *Bordetella bronchiseptica* and *B. pertussis*, possess CPS (*cap*) loci sharing 99% identity (Fig. 7*A*) possessing the characteristic *kpsMTED* genes for ABC transporter-dependent systems. However, these loci lack *vexE* and instead contain *kpsSC* genes suggesting a conventional assembly system producing a glycan with a terminal phosphatidylglycerol-linked β-Kdo oligosaccharide, like the classical *E. coli* "group 2" prototype (1). The precise glycan structures governed by the *cap* loci are unknown (50), but they encode homologs of TviBCDE (Fig. 7*A*), offering a possible explanation for published reports of *B. pertussis* cells reacting with polyclonal mouse antibodies raised against Vi antigen (51). *Bordetella* possess many virulence factors, which fall under the control of the Bvg two-component system that senses and reacts to the surrounding environment by regulating the transcription of hundreds of genes (52). *B. bronchiseptica* whole-cell lysates were examined from the virulent ($Bvg^+$) and avirulent ($Bvg^-$) phases (52), since basal Vi antibody reactivity (and *cap* gene expression) was previously reported in $Bvg^+$, with a substantial upregulation observed in $Bvg^-$ cells (51). In our hands, reactivity with anti-Vi-OAc antibody was indistinguishable between samples from the two Bvg phases, while the $Bvg^+$ sample reacted more strongly than the $Bvg^-$ sample with the polyclonal anti-Vi antibody (Fig. 7*B*). The reason for the difference in $Bvg^-$ phase reactivity, compared with published work, is unknown, but it was not pursued because it was not central to the goal of examining the activities of TviDE. As expected, deletion of the *cap* locus abolished reactivity with either antibody (Fig. 7*B*). These data indicate that the Vi-like similarities in the *cap*-encoded CPS of mammalian adapted *Bordetella* extend to both the glycan backbone and its *O*-acetylation.

TviD and TviE from *B. bronchiseptica* (referred to as $TviD_{Bb}$ and $TviE_{Bb}$) share 23% and 32% identity with the homologs from *S.* Typhi, respectively, and domain organizations are preserved. $TviD_{Bb}$ is proposed to have an N-terminal *O*-

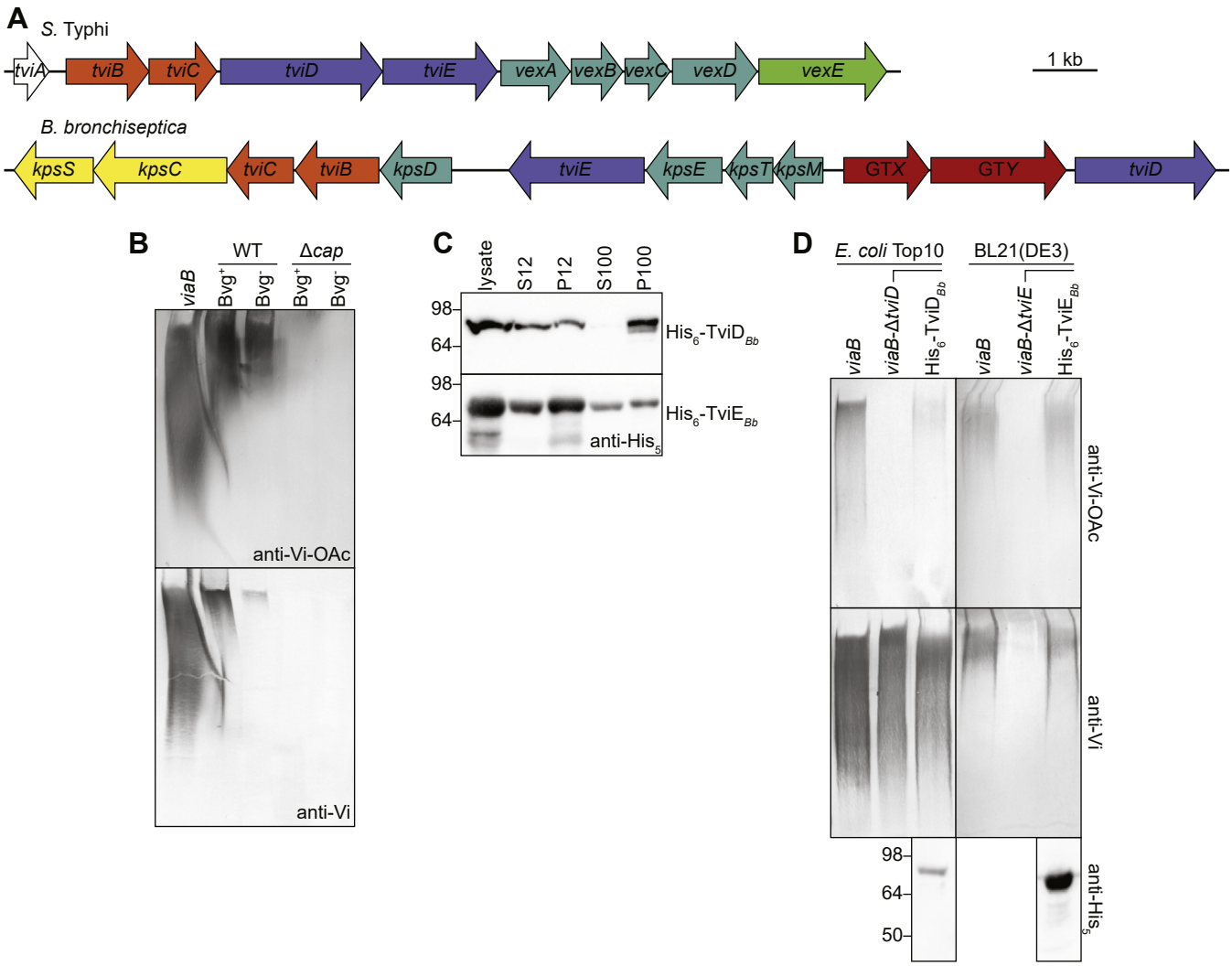


**Figure 7. Production of a Vi-related polysaccharide by *B. bronchiseptica* and participation of TviD and TviE from *B. bronchiseptica* with *S.* Typhi proteins in Vi antigen synthesis.** *A,* comparison of the genetic organization of the CPS loci from *S.* Typhi and *B. bronchiseptica*. *B, B. bronchiseptica* WT and *cap* locus deletion (Δ*cap*) cells were collected from $Bvg^+$ and $Bvg^-$ phase bacteria. Lysates were analyzed *via* Western immunoblots probed with anti-Vi-OAc and anti-Vi antibodies. *E. coli* Top10 harboring a plasmid containing *viaB* provides the positive control. *C,* cellular distribution of $His_6$-$TviD_{Bb}$ and $His_6$-$TviE_{Bb}$, expressed in *E. coli* Top10 and BL21(DE3), respectively. Protein was detected by Western immunoblots probed with anti-$His_5$ antibody. S12 and P12 are soluble and pellet fractions, respectively, from centrifugation at 12,000*g*, while S100 and P100 are the corresponding fractions obtained after centrifugation of the S12 fraction at 100,000*g*. The pH of the resuspension buffers used to analyze $His_6$-$TviD_{Bb}$ and $His_6$-$TviE_{Bb}$ was 6.7 and 7.7, respectively. *D,* Western immunoblots of proteinase K-digested whole-cell lysates showing the complementation of the *tviD* and *tviE*-deletions by expressing $His_6$-$TviD_{Bb}$ and $His_6$-$TviE_{Bb}$, respectively. Expression of the proteins was monitored by probing protein lysates with anti-$His_5$ antibody. Western immunoblots in (*C*) and (*D*) are representative of three biological replicates.

acetyltransferase domain, followed by a shorter TPR domain compared with TviD from *S.* Typhi, with only three repeats (Fig. S10*A*). The N-terminus of $TviD_{Bb}$ (residues 1–274) was modeled using RaptorX (43) and an SGNH hydrolase from the metagenome of Lake Arreo, Spain (PDB 5JD3) as a template (Fig. S10*B*). This template was also used to produce the third highest scoring model of TviD from *S.* Typhi using RaptorX (43). The residues determined to be catalytically important in TviD from *S.* Typhi (Cys18 and His253) are conserved in $TviD_{Bb}$, along with Asp250 in the DXXH motif (Fig. S10, *B* and *C*). The $TviE_{Bb}$ sequence predicts a C-terminal GT domain belonging to the GT4 family (Fig. S11*A*). A model of $TviE_{Bb}$, created using Phyre2 (34) and AtSus1 (PDB 3S29) as the template, resembles TviE from *S.* Typhi but possesses a larger, more complex, N-terminal domain (Fig. S11*B*). The catalytic site, including the important $EX_7E$ motif, is also conserved (Fig. S11, *B* and *C*).

To examine the properties of the *B. bronchiseptica* homologs, cellular fractionation was performed with *E. coli* Top10 and BL21(DE3) cells expressing $His_6$-$TviD_{Bb}$ and $His_6$-$TviE_{Bb}$, respectively. Samples from each fraction were analyzed by Western immunoblots with anti-$His_5$ antibodies and indicated similar cellular distribution to the *S.* Typhi homologs; $His_6$-$TviD_{Bb}$ localized to the membrane (P100) and $His_6$-$TviE_{Bb}$ was found in the soluble (S100) and membrane (P100) fractions (Fig. 7*C*). Since the early steps of Vi antigen biosynthesis differ in *S.* Typhi and *B. bronchiseptica*, the capacity of $His_6$-$TviD_{Bb}$ and $His_6$-$TviE_{Bb}$ to productively participate in the Vi antigen

biosynthesis machinery from *S.* Typhi was investigated by complementation experiments using *E. coli* Top10 and BL21(DE3) transformed with *viaB-ΔtviD* and *viaB-ΔtviE*, respectively. Immunoblots of the corresponding proteinase K-digested whole-cell lysates demonstrated that the *B. bronchiseptica* proteins were active in these backgrounds (Fig. 7*D*), although the amount of Vi antibody reactive material was reduced compared with that produced by the native proteins (compare to Figs. 2*D* and 4*D*). No conclusions were drawn about the relative amounts due to variables beyond protein structures, including different host and vector combinations.

## Discussion

The results described here show that TviD and TviE are an *O*-acetyltransferase belonging to the SGNH hydrolase family and a GT4 family GT for the biosynthesis of Vi antigen in *S.* Typhi and soil isolates of the Burkholderiaceae that include some *Bordetella* species, as well as Vi-related CPS (whose structure has not been elucidated) in mammalian-adapted *Bordetella* species. When combined with the enzymes for precursor formation, *S.* Typhi TviDE is sufficient for synthesis of *O*-acetylated Vi antigen.

The involvement of TviE as the sole GT required for Vi antigen biosynthesis indicates that this enzyme is a single catalytic site polymerase. There is precedent for GT4 family enzymes being able to add more than one glycosyl residues in the activity of PglH, a single active site processive polymerase from *C. jejuni* (32, 37). PglH adds precisely three GalNAc residues in biosynthesis of a heptasaccharide used for N-linked protein glycosylation, and it contains a molecular ruler to ensure fidelity (32). There is no comparable structure in TviE, as might be expected for an enzyme that generates much larger products. Polymerizing GTs may act on a glycose acceptor synthesized by one or more other GTs, as would be the case in a CPS with a terminal phosphatidylglycerol-linked β-Kdo oligosaccharide, which is implicated by the *cap* locus in *B. bronchiseptica*. In *S.* Typhi, the initiation reaction for Vi synthesis and the origin of the terminal diacyl-HexNAc have not yet been resolved, but proper acylation of the terminus by VexE is not required for polymerization (9). One attractive hypothesis is that *S.* Typhi TviE initiates polymerization using a sugar nucleotide acceptor. This strategy is used by cellulose synthase (BcsA), which has been studied in depth in *Rhodobacter sphaeroides* (53). Biosynthesis of cellulose occurs without the involvement of lipid-linked intermediates. The cellulose polymer is extended one glucose molecule at a time by BcsA (a GT2 enzyme). Growth of cellulose occurs at the nonreducing terminus, with the newly added glucose residue forming the acceptor for subsequent reactions (53). Another example is provided by the Class I bacterial hyaluronan synthase (HAS) from *Streptococcus equisimilis* (54). This enzyme initiates synthesis of chitin (oligo-GlcNAc) oligomers using UDP-GlcNAc as the initial acceptor and extends these oligosaccharides with the [3)-β-GlcNAc-(1→4)-β-GlcA-(1→] hyaluronan backbone (55). The mechanism by which this occurs has not been elucidated but addition occurs at the reducing terminus. The direction of Vi antigen growth has not been determined in *S.* Typhi, but the assembly system in which $TviE_{Bb}$ participates seems to make extension at the nonreducing end (building on the β-Kdo oligosaccharide) more likely. Our working hypothesis is that synthesis of Vi antigen begins on UDP-HexNAc prior to the sequential transfer of GalNAcA residues (from their UDP-linked precursor) to the nonreducing terminus. VexE would then acylate the reducing terminal GlcNAc residue during or postpolymerization.

TviE requires an $EX_7E$ motif for function like other GT4 proteins. Substitution of either Glu residue with Ala rendered TviE inactive without impacting protein solubility or stability. Like other GT4 enzymes, such as AtSus1, Ss2, SpsA, MshA, and PimB, TviE possesses basic residues within the active site to aid in the stabilization of the nucleotide sugar (35, 56–59). Arg406 and Lys411 are conserved among these enzymes and are involved in coordinating the pyrophosphate oxygens in the active site (Fig. S2).

Despite the lack of sequence homology to characterized *O*-acetyltransferases, TviD possesses an *O*-acetyltransferase domain belonging to the SGNH hydrolase family. Other members of this family, such as CsaC (MynC/SacC) and CssE (OatC), are involved in *O*-acetylation of CPS from *N. meningitidis* serogroups A and C, respectively (60, 61). Based on structural predictions, an SGNH hydrolase-like fold with an α/β/α core is found in the N-terminal part of TviD (Fig. 4*B*). Typically, Ser, Gly, Asn, His, and Asp/Glu are located within the catalytic core in conserved blocks, but as the SGNH family has grown, it is evident that some enzymes may lack these canonical residues (44). Most SGNH hydrolases possess a catalytic triad consisting of a Ser (nucleophile) from block I and a His and Asp (sometimes Glu) from block V (Fig. S6). An oxyanion hole is typically formed by the NH of the catalytic Ser from block I, the NH of Gly from block II, and the amide of Asn from block III (44). These residues hydrogen bond with the negatively charged intermediate, stabilizing the transition state (44). Multiple sequence alignments highlight the lack of sequence similarity shared by TviD and other representatives in regions of blocks II (NXSXXGXT) and III (GXND), and they align poorly in block I due to the presence in TviD of Gly-Ser-Cys instead of the typical Gly-Asp-Ser motif. Block V (DXXH) is conserved (Fig. S6). These features are conserved in $TviD_{Bb}$ (Fig. S10*C*). Although atypical, the Cys in block I and the His of block V are required for *O*-acetylation of Vi antigen by TviD (Fig. 4*D*). There is precedent for this type of arrangement provided by dienelactone hydrolase (Cys-His-Asp catalytic triad), and cysteine nucleophiles are commonly used by cysteine proteases in either a catalytic triad or dyad (47, 62, 63). *O*-acetylation was retained when the Asp of block V was replaced with Ala indicating that it is not essential for the activity of TviD (Fig. 4*D*). It is plausible that TviD has a Cys-His dyad. Asp is typically required to activate His, allowing it to deprotonate the nucleophile, but as Cys has a lower $pK_a$ than Ser, the Asp may not be essential (44). An extracellular lipase from *Streptomyces rimosus*, a member of the SGNH hydrolase family, is known to possess a Ser-His catalytic dyad,

although the mechanism has not been elucidated (64). Since blocks II and III are not conserved in TviD, it is challenging to identify the other residues, which compose the oxyanion hole in this enzyme, in the absence of a solved structure.

The C-terminal TPR domain of TviD is not essential for *O*-acetylation of Vi antigen but is required for membrane association and interaction with TviE. The function of the N-terminal α-helical domain of TviE offers a candidate for interaction, but this cannot be assessed because deletions of even a small part of this domain render TviE inactive *in vivo*. This part of the protein appears to be located away from the GT active site and may also be involved in protein–protein interactions. Unfortunately, attempts to get more insight into the stoichiometry of the complex by size-exclusion chromatography were unsuccessful. The $His_6$-TviDE-FLAG complex was found in a large single peak, calculated to be >600 kDa by interpolation from a standard curve (Fig. S12, *A* and *B*). The micelle size of LDAO is 17–22 kDa (65, 66), and monomeric $His_6$-TviD and TviE-FLAG are 96.8 kDa and 66.0 kDa, respectively, potentially suggesting a complex comprised of multiple copies of each protein, with higher levels of TviD:TviE (Fig. S12*C*). However, the elution profiles of individual $His_6$-TviD (Fig. S13*A*) and $His_6$-TviE (Fig. S13*B*) also showed large peaks of >600 kDa, so the contribution of aggregation cannot be excluded.

Although the removal of the TPR domains of TviD eliminates recruitment of TviE to the membrane and interactions between the proteins, this is not essential for *in vivo* synthesis of *O*-acetylated Vi antigen, under conditions where the truncated TviD protein is overexpressed. Nevertheless, evidence does exist for a functional complex coupling synthesis and export in the cell. During synthesis, Vi antigen is protected from cytoplasmic expression of a Vi antigen depolymerase enzyme (11). This would allow efficient integration of synthesis and *O*-acetylation. Notably, the VexE acyltransferase also contains a TPR domain (10 repeats) at the N-terminus of the protein (9, 41, 42), suggesting that it could also participate in a larger complex. The importance of TPR motifs is established for some other exported polysaccharides in Gram-negative bacteria; examples include alginate, cellulose, poly-β-(1,6)-*N*-acetyl-D-glucosamine (PNAG), and Pel (67). In these examples, the TPR-containing enzymes reside in the periplasm and act as a scaffold, coordinating various interactions. In the PNAG, Pel, and cellulose systems, the TPR-containing proteins have an additional domain, which facilitates polymer export across the outer membrane. In alginate, outer membrane export is completed by a separate protein, which interacts with the TPR-containing protein. The TPR domain has also been shown to interact with polymer-modifying enzymes (67). These data support the hypothesis that the TPR domain may guide some polymers to the export protein during synthesis (67). We cannot exclude further roles like this for the TPR motifs beyond protein–protein interactions in Vi antigen production.

The *cap* loci of *B. pertussis* and *B. bronchiseptica* are 99% identical, and studies on *B. pertussis* determined that CPS genes are not upregulated during the $Bvg^+$ phase of the bacteria (51). However, *B. pertussis* lacking *kpsT* (the gene that encodes the nucleotide-binding domain of the ABC transporter) was drastically attenuated *in vivo* due to the downregulation of virulence genes, so the precise role played by CPS is uncertain (68). Moderate attenuation occurred when *tviC* was deleted, suggesting that only the CPS export machinery plays a critical role in virulence (68). The structure of the glycan product directed by the *cap* locus is unknown, but antibody reactivity shown here and reported previously (51), together with the functional studies of the TviDE homologs from *B. bronchiseptica*, supports the presence of a glycan resembling (or sharing epitopes with) Vi antigen. The involvement of the TviE homologs in two different polymerization contexts is interesting (and perhaps surprising) and merits further investigation. Unraveling the mechanistic underpinnings will depend on establishing *in vitro* systems and (potentially) structures of the enzymes. In addition to genes correlated with Vi antigen synthesis in *S.* Typhi and ABC transporter-dependent CPS export, the *cap* loci also contain genes encoding two putative GTs (arbitrarily designated GT*X* and GT*Y* here) (Fig. 7*A*). By analogy to proposals for related systems in other bacteria (1), at least one GT is anticipated to be required to transition from the β-Kdo oligosaccharide (formed by KpsSC) to the repeat-unit domain of CPS, which is expected to be polymerized and *O*-acetylated by TviE and TviD, respectively. One of the unassigned GTs might participate in modifying a Vi antigen backbone. This seems likely with the Vi-epitopes still available but can only be resolved with a fully elucidated carbohydrate structure. The information described here provides a foundation for such investigations.

## Experimental procedures

### Bacterial strains and growth conditions

The strains used in this study were *E. coli* Top10 ($F^-$, *mcrA*, Δ(*mrr-hsdRMS-mcrBC*), φ80, *lacZ*ΔM15, Δ*lacX74*, *deoR*, *nupG*, *recA1*, *araD139*, Δ(*ara-leu*)7697, *galU*, *galK*, *rpsL*($Str^r$), *endA1*) (Invitrogen), *E. coli* BL21(DE3) ($F^-$ *ompT gal dcm lon* $hsdS_B(r_B^-m_B^-)$ λ(DE3[*lacI lacUV5-T7p07 ind1 sam7 nin5*]) $[malB^+]_{K\text{-}12}(\lambda^S)$) (Invitrogen), CWG1238 (*S.* Typhi H251.1 Δ*waaG::kan;* $Km^r$) (9), and *B. bronchiseptica* RB50 (50). *E. coli* and *S.* Typhi were routinely grown at 37 °C in lysogeny broth (LB) supplemented with the appropriate antibiotic (100 μg $mL^{-1}$ ampicillin, 34 μg $mL^{-1}$ chloramphenicol, 50 μg $mL^{-1}$ kanamycin, or 10 μg $mL^{-1}$ tetracycline) and 100 μg $mL^{-1}$ 2,3-dihydroxybenzoic acid when necessary (CWG1238). *B. bronchiseptica* RB50 was grown at 37 °C in LB ($Bvg^+$ phase) or LB supplemented with 50 mM $MgSO_4$ ($Bvg^-$ phase). In *B. bronchiseptica*, the capsule locus deletion mutant (Δ*cap*) was constructed by replacing the entire locus except the 3′ half of *kpsS* and *tviD* with a kanamycin resistance cassette, using an approach as described previously (69).

### General DNA methods

The plasmids used in this study are described in Table S1. Plasmid DNA was purified using the PureLink Quick (Invitrogen) or GeneJET (Thermo Fisher) Plasmid Miniprep kit.

DNA fragments amplified by PCR or obtained from restriction endonuclease digests were purified using PureLink (Invitrogen) or GeneJET (Thermo Fisher) PCR purification kits. Restriction endonucleases, T4 DNA ligase, and Gibson Assembly mix (NEB) were used according to the manufacturer's instructions. Amino acid insertions and substitutions were generated using the QuikChange protocol (Agilent) for site-directed mutagenesis with KOD Hot Start DNA polymerase (EMD Millipore). The Q5 site-directed mutagenesis protocol (NEB) was followed for the generation of TviD$^{1-322}$ using PaCeR polymerase (GeneBio Systems, Inc.). Gene deletions were generated in pWQ783 using inverse PCR with either KOD Hot Start (EMD Millipore) or Phusion High-fidelity (NEB) DNA polymerase. Primers for inverse PCR were synthesized with a 5′-phosphate to facilitate the ligation of the linear product. Custom oligonucleotide primers used in this study were purchased from Sigma and Integrated DNA Technologies (Table S2). All constructs were confirmed *via* DNA sequencing at the Advanced Analysis Center at the University of Guelph.

### Protein expression, cellular fractionation, and purification

Overnight bacterial cultures were diluted 1:50 into LB supplemented with the appropriate antibiotic. Prior to inducing protein expression, cultures were grown to an $OD_{600}$ of 0.5. Protein expression in *E. coli* Top10 containing pBAD plasmids was induced using L-arabinose (0.02% [w/v]) or isopropyl-β-D-thiogalactopyranoside (0.5 mM) for *E. coli* BL21(DE3) containing pET constructs. Cultures were transferred to 18 °C and growth continued for an additional 16 h. Cells were then collected by centrifugation at 5000*g* for 20 min at 4 °C and resuspended in 50 ml of resuspension buffer, containing one cOmplete Mini EDTA-free protease inhibitor tablet (Roche Applied Science). The resuspension buffer (50 mM Tris, 250 mM NaCl) was used with different pH values depending on the protein being analyzed, and these are indicated in relevant figure legends. The cells were lysed by passage through an EmulsiFlex-C3 (Avestin) at 15,000 psi. Unbroken cells and large debris (P12 fraction) were removed by centrifugation at 12,000*g* for 20 min at 4 °C, and the supernatant (S12 fraction) was separated into membranes (P100) and soluble fractions (S100) by centrifugation at 100,000*g* for 1 h at 4 °C. To extract membrane-associated $His_6$-TviD, the membrane pellet (P100) was resuspended in 20 ml of resuspension buffer containing 1% (v/v) LDAO (Sigma) and incubated overnight with rocking at 4 °C. Insoluble material was removed by centrifugation at 100,000*g* for 1 h at 4 °C. The supernatant, containing solubilized $His_6$-TviD, was used in the subsequent purification steps with the buffers containing 0.1% (v/v) LDAO. To purify soluble (or solubilized) proteins, samples were loaded on an IMAC gravity column containing 2 ml of Ni-NTA agarose resin (Qiagen). The matrix was washed successively with ten column volumes of each wash buffer (specified in the relevant figure legends), before the protein was eluted with five column volumes of resuspension buffer containing 300 mM imidazole. The eluted protein was buffer exchanged using a PD-10 desalting column (GE Healthcare) into imidazole-free resuspension buffer with 150 mM NaCl (containing 0.1% [v/v] LDAO for detergent-solubilized proteins). The protein was then concentrated using a Vivaspin6 10 kDa, 30 kDa, or 50 kDa MWCO column (Sartorius), depending on the size of the protein. The folding state of purified proteins was assessed by using the Protein Thermal Shift Dye kit (Thermo Fisher) in combination with a StepOnePlus Real-Time PCR System (ThermoFisher), according to the manufacturer's instructions. To examine the cellular distribution of epitope-tagged proteins, samples of the lysate, S12, P12, S100, and P100 fractions were separated by SDS-PAGE and subjected to Western immunoblotting.

### Analysis of potential TviDE complexes

To examine potential interactions between TviD and TviE, $His_6$-TviDE-FLAG or $His_6$-TviD$^{1-322}$E-FLAG was expressed in *E. coli* Top10 transformed with plasmids pWQ1059 or pWQ1060, respectively, and P100 and S100 fractions were prepared as described above. $His_6$-TviD$^{1-322}$E-FLAG is present in the soluble fraction (S100), while $His_6$-TviDE-FLAG is membrane-associated and was solubilized with LDAO. To purify putative protein complexes, the column matrix was washed consecutively with 20 column volumes of each wash buffer prior to protein elution. Samples from each step in the process were collected for analysis using SDS-PAGE and Western immunoblotting.

For gel-filtration chromatography, $His_6$-TviD, $His_6$-TviE (pWQ1065), and $His_6$-TviDE-FLAG eluted from Ni-NTA columns were buffer exchanged using a PD-10 desalting column (GE Healthcare) into 50 mM Tris, 150 mM NaCl, pH 7.4, 0.1% (v/v) LDAO. The samples were then concentrated to approximately 5 mg mL$^{-1}$ using either a Vivaspin6 30 kDa ($His_6$-TviE and $His_6$-TviDE-FLAG) or 50 kDa ($His_6$-TviD) MWCO column (Satorius). Samples were analyzed using an ÄKTA Pure FLPC equipped with a Superdex 200 Increase 10/300 Gl column (GE Healthcare). Gel-filtration chromatography was carried out in the same buffer as the loaded sample, and the absorbance was monitored at 280 nm during elution. Fractions containing $His_6$-TviDE-FLAG were collected and concentrated using a Vivaspin6 30 kDa MWCO column (Satorius), and 5 μg samples were examined by SDS-PAGE and Western immunoblotting.

### SDS-PAGE and Western immunoblotting

Samples consisted of purified polysaccharides (see below) or whole-cell lysates. To analyze Vi antigen in lysates, cells corresponding to 1 optical density ($OD_{600}$) unit-equivalent were collected by centrifugation, and whole-cell lysates were prepared by proteinase K-digestion (70). To detect protein expression, lysates were prepared in the absence of proteinase K. Samples were routinely heated at 100 °C for 10 min prior to SDS-PAGE. However, detection of membrane-associated TviD

was an exception, where samples were prepared following the protocol described previously (71) and incubated at 37 °C for 30 min. All samples were separated using SDS-PAGE with 10% resolving gels. For detection of Vi antigen by Western immunoblotting, samples were transferred to positively charged nylon membranes (Biodyne B; Pall) at 250 mA for 1 h. Proteins were transferred to nitrocellulose membranes (Protran; GE Healthcare) using the Power Blotter Semi-dry transfer system (Thermo Fisher). The antibodies used to detect Vi antigens were murine monoclonal anti-Vi-OAc antibody P2B1G2/A9 ((25); diluted 1:300) or polyclonal anti-Vi antibody (BD Difco; diluted 1:350). The secondary antibodies were alkaline phosphatase-conjugated goat anti-mouse (Cedarlane; diluted 1:3000) or anti-rabbit secondary antibodies (Cedarlane; diluted 1:3000). Immunoblots were developed using 5-bromo-4-chloro-3-indoyl phosphate and nitroblue tetrazolium (Roche Applied Science). Epitope-tagged proteins were detected using either murine monoclonal anti-FLAG (Sigma; diluted 1:1000), murine monoclonal anti-pentahistidine ($His_5$) (Qiagen; diluted 1:2000), and the secondary antibody was horseradish-peroxidase-conjugated goat anti-mouse (Cedarlane; diluted 1:3000). Detection was accomplished using the HRP-substrate Luminata Crescendo (EMD Millipore). Molecular weight determination was performed using Image Lab 6.0.1 software (BioRad).

### Purification of and NMR analysis of Vi antigen

The method for purifying native exported CPS from *E. coli* CWQ1238 has been described elsewhere (9). Large-scale purification of internal Vi antigen was achieved using a modification of the published method (9). Twelve-liter LB cultures, supplemented with the appropriate antibiotic(s), were inoculated (1:100) from overnight cultures of *E. coli* Top10 transformed with plasmids encoding TviABCDE (pWQ1043), TviABCE (pWQ1046), or TviABCE[$His_6$-TviD] (pWQ1052). The first two of these were grown at 37 °C for 16 h, while the latter was grown following the induction protocol described above for expressing the recombinant proteins. Cells were collected by centrifugation (5000*g* for 20 min) and lyophilized. The dried cell pellet was resuspended in 50 ml of 50 mM Tris buffer (pH 8.0) containing 5 mM EDTA and 2 mg $mL^{-1}$ lysozyme (Sigma). The mixture was stirred for 16 h at 4 °C and then diluted to a final volume of 100 ml by adding 50 mM Tris buffer (pH 8.0) containing 5 mM EDTA, 10 mM $MgCl_2$, and 1 μg $mL^{-1}$ each of DNAse, and RNAse (Roche Applied Science). The digestion of DNA and RNA was proceeded with stirring for 1 h at 37 °C. An equal volume of 90% aqueous phenol was added to the preparation, and the mixture was stirred for 1 h at 70 °C. The mixture was then cooled on ice for 20 min to bring the temperature below 15 °C, and phase separation was achieved by centrifugation at 10,000*g* for 20 min. The aqueous phase was collected, placed in a 3.5 kDa MWCO dialysis membrane (Spectrum Labs), and dialyzed against water for 2 days. Finally, the sample was centrifuged at 100,000*g* for 16 h, and the supernatant was retained and lyophilized.

NMR analysis was performed on intracellular Vi antigen, and the spectra were compared with native and chemically de-*O*-acetylated native CPS obtained by base treatment with ammonium hydroxide, as described (9). The inherent viscosity of native Vi antigen results in spectra with broad peaks in NMR spectra, so data were collected for a modified polysaccharide obtained by solvolysis with trifluoroacetic acid (TFA). Seventy-five milligram samples of purified polysaccharide were resuspended in 500 μl of 99% TFA and incubated at 100 °C for 2 h. After solvolysis, TFA was evaporated using nitrogen gas. The dried material was resuspended in water and lyophilized twice before resuspending in 1 ml of water. The sample was then loaded onto a Sephadex G-50 superfine column (2.5 × 75 cm) eluted with 1% (v/v) acetic acid and 0.4% (v/v) pyridine with a flow rate of 0.6 ml $min^{-1}$, and the elution was monitored using a Smartline 2300 refractive index detector (Knauer). The modified polysaccharide eluted immediately after the void volume of the column was collected, concentrated using a rotary evaporator, and lyophilized. The samples were deuterium-exchanged by freeze-drying twice with 99.9% $D_2O$, resuspended in 250 μl of 99.9% $D_2O$, and placed in a 5-mm Shigemi NMR microtube. $^1H$, $^{13}C$ NMR, and two-dimensional $^1H$, $^{13}C$ heteronuclear single-quantum coherence (HSQC) spectra were obtained at 25 °C using a Bruker Avance III 600-MHz spectrometer equipped with a 5 mm TCI cryoprobe, located in the NMR Centre of the Advanced Analysis Centre at the University of Guelph. Sodium 3-trimethylsilylpropanoate-2,2,3,3-*d*4 was used as an internal chemical shift reference ($\delta_H$ = 0 ppm, $\delta_C$ = −1.6 ppm).

### Immunofluorescence microscopy

Immunofluorescence microscopy was performed on fixed cells to examine the localization of Vi antigen, following published protocols (71, 72). Overnight cultures of *E. coli* Top10 transformants were diluted 1:50 in 5 ml of LB supplemented with the appropriate antibiotics and L-arabinose, where induction of recombinant proteins was required. Cultures were grown at 37 °C until an $OD_{600}$ of 0.5 was reached, at which time 1 $OD_{600}$ unit-equivalent of cells was collected by centrifugation (5000*g* for 10 min). The cells were resuspended in 1 ml of 5% (v/v) formaldehyde and incubated at room temperature for 1 h. The fixed cells were collected by centrifugation and washed twice with 1 ml of phosphate-buffered saline (PBS), prior to resuspension in 50 μl of PBS. Glass microscope slides were coated with poly-L-lysine, and 10 μl samples were added to each well. The slides were incubated at room temperature for 10 min. Permeabilization of cells was used to visualize intracellular Vi antigen and was accomplished by adding 10 μl of 0.5 mg $mL^{-1}$ lysozyme (in 25 mM Tris, 10 mM EDTA, pH 8) and 0.1% Triton X-100 (in PBS), separately, with 15 min incubation for each. The wells were then blocked with 1% (w/v; in PBS) bovine serum albumin (BSA) for 15 min. Following blocking, the slides were treated with either murine anti-Vi-OAc antibody P2B1G2/A9 (25) or rabbit anti-Vi antibody (BD Difco) diluted 1:100 in 1% BSA. After

incubation at room temperature for 30 min, the unbound primary antibody was removed by washing three times. The secondary fluorescein isothiocyanate (FITC)-conjugated goat anti-mouse (Sigma) or anti-rabbit (Sigma) antibodies were diluted 1:250 in 1% BSA, added to the wells, and the slides were incubated for 30 min in the dark at room temperature. Finally, the slides were then washed and mounted in Vectashield (Vector Laboratories). Images were obtained using an inverted Leica DMi8 microscope connected to a Quorum Diskovery Spinning Disk system (Quorum Technologies Inc.) and processed using Volocity software (version 6.3; PerkinElmer) in the University of Guelph Advanced Analysis Centre.

## Data availability

The authors declare that all data are contained within the manuscript and supporting information.

*Supporting information*—This article contains supporting information (9, 28, 34, 41–43, 73–75).

*Acknowledgments*—We thank Dr Ayub Qadri for the P2B1G2/A9 Vi antigen antibody, Dr Sean Liston for purified native and de-*O*-acetylated Vi antigen samples, as well as assistance with the Vi antigen purification method, Dr Cezar Khursigara for the goat anti-rabbit FITC antibody, and Dr Bradley Clarke for reviewing and commenting on the manuscript draft.

*Author contributions*—S. W. and C. W. conceptualization; C. W. funding acquisition; S. W., C. S., and O. G. O. investigation; A. P. resources; C. W. supervision; S. W. writing—original draft; S. W., C. S., O. G. O., A. P., and C. W. writing—review and editing

*Funding and additional information*—This research was funded by the Canadian Institutes of Health Research (CIHR) Foundation Grant program (to C. W.). C. W. is the recipient of a Canada Research Chair and C. S. received a CIHR Doctoral Fellowship.

*Conflicts of interest*—The authors declare that they have conflicts of interest with the contents of this article.

*Abbreviations*—The abbreviations used are: ABC, ATP-binding cassette; CPS, capsular polysaccharide; GT, glycosyltransferase; NDP, nucleoside diphosphate; OPX, outer membrane polysaccharide export; PBS, phosphate-buffered saline; PCP-3, polysaccharide copolymerase family 3.

## References

1. Whitfield, C., Wear, S. S., and Sande, C. (2020) Assembly of bacterial capsular polysaccharides and exopolysaccharides. *Annu. Rev. Microbiol.* **74**, 521–543
2. Taylor, C., and Roberts, I. (2005) Capsular polysaccharides and their role in virulence. *Contrib. Microbiol.* **12**, 55–66
3. Willis, L. M., and Whitfield, C. (2013) Structure, biosynthesis, and function of bacterial capsular polysaccharides synthesized by ABC transporter-dependent pathways. *Carbohydr. Res.* **378**, 35–44
4. Willis, L. M., Stupak, J., Richards, M. R., Lowary, T. L., Li, J., and Whitfield, C. (2013) Conserved glycolipid termini in capsular polysaccharides synthesized by ATP-binding cassette transporter-dependent pathways in Gram-negative pathogens. *Proc. Natl. Acad. Sci. U. S. A.* **110**, 7868–7873
5. Ovchinnikova, O. G., Doyle, L., Huang, B.-S., Kimber, M. S., Lowary, T. L., and Whitfield, C. (2016) Biochemical characterization of bifunctional 3-deoxy-β-D-*manno*-oct-2-ulosonic acid (β-Kdo) transferase KpsC from *Escherichia coli* involved in capsule biosynthesis. *J. Biol. Chem.* **291**, 21519–21530
6. Doyle, L., Ovchinnikova, O. G., Myler, K., Mallette, E., Huang, B.-S., Lowary, T. L., Kimber, M. S., and Whitfield, C. (2019) Biosynthesis of a conserved glycolipid anchor for Gram-negative bacterial capsules. *Nat. Chem. Biol.* **15**, 632–640
7. Lanz, N. D., Ming, S. A., Thon, V., Veeramachineni, V. M., Azurmendi, H. F., and Vann, W. F. (2021) Characterization of the *β*-KDO transferase KpsS, the initiating enzyme in the biosynthesis of the lipid acceptor for *Escherichia coli* polysialic acid. *Biochemistry* **60**, 2044–2054
8. Willis, L. M., and Whitfield, C. (2013) KpsC and KpsS are retaining 3-deoxy-D-*manno*-oct-2-ulosonic acid (Kdo) transferases involved in synthesis of bacterial capsules. *Proc. Natl. Acad. Sci. U. S. A.* **110**, 20753–20758
9. Liston, S. D., Ovchinnikova, O. G., and Whitfield, C. (2016) Unique lipid anchor attaches Vi antigen capsule to the surface of *Salmonella enterica* serovar Typhi. *Proc. Natl. Acad. Sci. U. S. A.* **113**, 6719–6724
10. Snellings, N. J., Johnson, E. M., Kopecko, D. J., Collins, H. H., and Baron, L. S. (1981) Genetic regulation of variable Vi antigen expression in a strain of *Citrobacter freundii*. *J. Bacteriol.* **145**, 1010–1017
11. Liston, S. D., McMahon, S. A., Le Bas, A., Suits, M. D. L., Naismith, J. H., and Whitfield, C. (2018) Periplasmic depolymerase provides insight into ABC transporter-dependent secretion of bacterial capsular polysaccharides. *Proc. Natl. Acad. Sci. U. S. A.* **115**, E4870–E4879
12. Gross, R., Guzman, C. A., Sebaihia, M., Martins dos Santos, V. A. P., Pieper, D. H., Koebnik, R., Lechner, M., Bartels, D., Buhrmester, J., Choudhuri, J. V., Ebensen, T., Gaigalat, L., Herrmann, S., Khachane, A. N., Larisch, C., *et al.* (2008) The missing link: *Bordetella petrii* is endowed with both the metabolic versatility of environmental bacteria and virulence traits of pathogenic Bordetellae. *BMC Genomics* **9**, 449
13. Heyns, K., and Kiessling, G. (1967) Strukturaufklärung des Vi-antigens aus *Citrobacter freundii* (*E. coli*) 5396/38. *Carbohydr. Res.* **3**, 340–353
14. Daniels, E. M., Schneerson, R., Egan, W. M., Szu, S. C., and Robbins, J. B. (1989) Characterization of the *Salmonella* paratyphi C Vi polysaccharide. *Infect. Immun.* **57**, 3159–3164
15. Keestra-Gounder, A. M., Tsolis, R. M., and Bäumler, A. J. (2015) Now you see me, now you don't: The interaction of *Salmonella* with innate immune receptors. *Nat. Rev. Microbiol.* **13**, 206–216
16. Hone, D. M., Attridge, S. R., Forrest, B., Morona, R., Daniels, D., LaBrooy, J. T., Bartholomeusz, R. C. A., Shearman, D. J. C., and Hackett, J. (1988) A *galE* via (Vi antigen-negative) mutant of *Salmonella* typhi Ty2 retains virulence in humans. *Infect. Immun.* **56**, 1326–1333
17. Crawford, R. W., Wangdi, T., Spees, A. M., Xavier, M. N., Tsolis, R. M., and Bäumler, A. J. (2013) Loss of very-long O-antigen chains optimizes capsule-mediated immune evasion by *Salmonella enterica* serovar Typhi. *MBio* **4**. e00232-13
18. Wilson, R. P., Winter, S. E., Spees, A. M., Winter, M. G., Nishimori, J. H., Sanchez, J. F., Nuccio, S.-P., Crawford, R. W., Tükel, Ç., and Bäumler, A. J. (2011) The Vi capsular polysaccharide prevents complement receptor 3-mediated clearance of *Salmonella enterica* serotype Typhi. *Infect. Immun.* **79**, 830–837
19. Kantele, A., Pakkanen, S. H., Karttunen, R., and Kantele, J. M. (2013) Head-to-head comparison of humoral immune responses to Vi capsular polysaccharide and *Salmonella* Typhi Ty21a typhoid vaccines-a randomized trial. *PLoS One* **8**, e60583
20. Klugman, K. P., Koornhof, H. J., Schneerson, R., Cadoz, M., Gilbertson, I. T., Robbins, J. B., Schulz, D., and Armand, J. (1987) Protective activity of Vi capsular polysaccharide vaccine against typhoid fever. *Lancet* **2**, 1165–1169
21. Szewczyk, B., and Taylor, A. (1980) Immunochemical properties of Vi antigen from *Salmonella* typhi Ty2: Presence of two antigenic determinants. *Infect. Immun.* **29**, 539–544

22. Virlogeux, I., Waxin, H., Ecobichon, C., and Popoff, M. Y. (1995) Role of the *viaB* locus in synthesis, transport and expression of *Salmonella* typhi Vi antigen. *Microbiology* **141**, 3039–3047
23. Wetter, M., Goulding, D., Pickard, D., Kowarik, M., Waechter, C. J., Dougan, G., and Wacker, M. (2012) Molecular characterization of the *viaB* locus encoding the biosynthetic machinery for Vi capsule formation in *Salmonella* Typhi. *PLoS One* **7**, e45609
24. Zhang, H., Zhou, Y., Bao, H., and Liu, H.-W. (2006) Vi antigen biosynthesis in *Salmonella* typhi: Characterization of UDP-*N*-acetylglucosamine C-6 dehydrogenase (TviB) and UDP-*N*-acetylglucosaminuronic acid C-4 epimerase (TviC). *Biochemistry* **45**, 8163–8173
25. Qadri, A., Ghosh, S., and Talwar, G. P. (1990) Monoclonal antibodies against two discrete determinants on Vi capsular polysaccharide. *J. Immunoassay.* **11**, 235–250
26. Sychantha, D., Brott, A. S., Jones, C. S., and Clarke, A. J. (2018) Mechanistic pathways for peptidoglycan O-acetylation and de-O-acetylation. *Front. Microbiol.* **9**, 2332
27. Lombard, V., Golaconda Ramulu, H., Drula, E., Coutinho, P. M., and Henrissat, B. (2014) The carbohydrate-active enzymes database (CAZy) in 2013. *Nucleic Acids Res.* **42**, D490–D495
28. Marchler-Bauer, A., Bo, Y., Han, L., He, J., Lanczycki, C. J., Lu, S., Chitsaz, F., Derbyshire, M. K., Geer, R. C., Gonzales, N. R., Gwadz, M., Hurwitz, D. I., Lu, F., Marchler, G. H., Song, J. S., *et al.* (2017) CDD/SPARCLE: Functional classification of proteins via subfamily domain architectures. *Nucleic Acids Res.* **45**, D200–D203
29. Martinez-Fleites, C., Proctor, M., Roberts, S., Bolam, D. N., Gilbert, H. J., and Davies, G. J. (2006) Insights into the synthesis of lipopolysaccharide and antibiotics through the structures of two retaining glycosyltransferases from family GT4. *Chem. Biol.* **13**, 1143–1152
30. Guerin, M. E., Kordulakova, J., Schaeffer, F., Svetlikova, Z., Buschiazzo, A., Giganti, D., Gicquel, B., Mikusova, K., Jackson, M., and Alzari, P. M. (2007) Molecular recognition and interfacial catalysis by the essential phosphatidylinositol mannosyltransferase PimA from mycobacteria. *J. Biol. Chem.* **282**, 20705–20714
31. Liston, S. D., Clarke, B. R., Greenfield, L. K., Richards, M. R., Lowary, T. L., and Whitfield, C. (2015) Domain interactions control complex formation and polymerase specificity in the biosynthesis of the *Escherichia coli* O9a antigen. *J. Biol. Chem.* **290**, 1075–1085
32. Ramírez, A. S., Boilevin, J., Mehdipour, A. R., Hummer, G., Darbre, T., Reymond, J.-L., and Locher, K. P. (2018) Structural basis of the molecular ruler mechanism of a bacterial glycosyltransferase. *Nat. Commun.* **9**, 445
33. Lairson, L. L., Henrissat, B., Davies, G. J., and Withers, S. G. (2008) Glycosyltransferases: Structures, functions, and mechanisms. *Annu. Rev. Biochem.* **77**, 521–555
34. Kelley, L. A., Mezulis, S., Yates, C. M., Wass, M. N., and Sternberg, M. J. E. (2015) The Phyre2 web portal for protein modeling, prediction and analysis. *Nat. Protoc.* **10**, 845–858
35. Zheng, Y., Anderson, S., Zhang, Y., and Garavito, R. M. (2011) The structure of sucrose synthase-1 from *Arabidopsis thaliana* and its functional implications. *J. Biol. Chem.* **286**, 36108–36118
36. Kostova, Z., Yan, B. C., Vainauskas, S., Schwartz, R., Menon, A. K., and Orlean, P. (2003) Comparative importance *in vivo* of conserved glutamate residues in the $EX_7E$ motif retaining glycosyltransferase Gpi3p, the UDP-GlcNAc-binding subunit of the first enzyme in glycosylphosphatidylinositol assembly. *Eur. J. Biochem.* **270**, 4507–4514
37. Troutman, J. M., and Imperiali, B. (2009) *Campylobacter jejuni* PglH is a single active site processive polymerase that utilizes product inhibition to limit sequential glycosyl transfer reactions. *Biochemistry* **48**, 2807–2816
38. Cid, E., Gomis, R. R., Geremia, R. A., Guinovart, J. J., and Ferrer, J. C. (2000) Identification of two essential glutamic acid residues in glycogen synthase. *J. Biol. Chem.* **275**, 33614–33621
39. Greenfield, L. K., Richards, M. R., Vinogradov, E., Wakarchuk, W. W., Lowary, T. L., and Whitfield, C. (2012) Domain organization of the polymerizing mannosyltransferases involved in synthesis of the *Escherichia coli* O8 and O9a lipopolysaccharide O-antigens. *J. Biol. Chem.* **287**, 38135–38149
40. Altschul, S. F., Madden, T. L., Schäffer, A. A., Zhang, J., Zhang, Z., Miller, W., and Lipman, D. J. (1997) Gapped BLAST and PSI-BLAST: A new generation of protein database search programs. *Nucleic Acids Res.* **25**, 3389–3402
41. Zimmermann, L., Stephens, A., Nam, S.-Z., Rau, D., Kübler, J., Lozajic, M., Gabler, F., Söding, J., Lupas, A. N., and Alva, V. (2018) A completely reimplemented MPI bioinformatics toolkit with a new HHpred server at its core. *J. Mol. Biol.* **430**, 2237–2243
42. Karpenahalli, M. R., Lupas, A. N., and Söding, J. (2007) TPRpred: A tool for prediction of TPR-, PPR- and SEL1-like repeats from protein sequences. *BMC Bioinformatics* **8**, 2
43. Källberg, M., Wang, H., Wang, S., Peng, J., Wang, Z., Lu, H., and Xu, J. (2012) Template-based protein structure modeling using the RaptorX web server. *Nat. Protoc.* **7**, 1511–1522
44. Akoh, C. C., Lee, G.-C., Liaw, Y.-C., Huang, T.-H., and Shaw, J.-F. (2004) GDSL family of serine esterases/lipases. *Prog. Lipid Res.* **43**, 534–552
45. Riley, L. M., Weadge, J. T., Baker, P., Robinson, H., Codée, J. D. C., Tipton, P. A., Ohman, D. E., and Howell, P. L. (2013) Structural and functional characterization of *Pseudomonas aeruginosa* AlgX: Role of AlgX in alginate acetylation. *J. Biol. Chem.* **288**, 22299–22314
46. Jones, C. S., Sychantha, D., Howell, P. L., and Clarke, A. J. (2020) Structural basis for the *O*-acetyltransferase function of the extracytoplasmic domain of OatA from *Staphylococcus aureus*. *J. Biol. Chem.* **295**, 8204–8213
47. Gariev, I. A., and Varfolomeev, S. D. (2006) Hierarchical classification of hydrolases catalytic sites. *Bioinformatics* **22**, 2574–2576
48. Gautier, R., Douguet, D., Antonny, B., and Drin, G. (2008) HELIQUEST: A web server to screen sequences with specific α-helical properties. *Bioinformatics* **24**, 2101–2102
49. D'Andrea, L. D., and Regan, L. (2003) TPR proteins: The versatile helix. *Trends Biochem. Sci.* **28**, 655–662
50. Parkhill, J., Sebaihia, M., Preston, A., Murphy, L. D., Thomson, N., Harris, D. E., Holden, M. T. G., Churcher, C. M., Bentley, S. D., Mungall, K. L., Cerdeño-Tárraga, A. M., Temple, L., James, K., Harris, B., Quail, M. A., *et al.* (2003) Comparative analysis of the genome sequences of *Bordetella pertussis, Bordetella parapertussis* and *Bordetella bronchiseptica*. *Nat. Genet.* **35**, 32–40
51. Neo, Y., Li, R., Howe, J., Hoo, R., Pant, A., Ho, S., and Alonso, S. (2010) Evidence for an intact polysaccharide capsule in *Bordetella pertussis*. *Microbes Infect.* **12**, 238–245
52. Cotter, P. A., and Miller, J. F. (2001) Bordetella. In: Groisman, E. A., ed. *Principles of Bacterial Pathogenesis*, Academic Press, San Diego, CA: 619–674
53. Morgan, J. L. W., McNamara, J. T., Fischer, M., Rich, J., Chen, H.-M., Withers, S. G., and Zimmer, J. (2016) Observing cellulose biosynthesis and membrane translocation *in crystallo*. *Nature* **531**, 329–334
54. Weigel, P. H., West, C. M., Zhao, P., Wells, L., Baggenstoss, B. A., and Washburn, J. L. (2015) Hyaluronan synthase assembles chitin oligomers with -GlcNAc(α1→)UDP at the reducing end. *Glycobiology* **25**, 632–643
55. Weigel, P. H., Baggenstoss, B. A., and Washburn, J. L. (2017) Hyaluronan synthase assembles hyaluronan on a $[GlcNAc(\beta1,4)]_n$-GlcNAc(α1→)UDP primer and hyaluronan retains this residual chitin oligomer as a cap at the nonreducing end. *Glycobiology* **27**, 536–554
56. Vetting, M. W., Frantom, P. A., and Blanchard, J. S. (2008) Structural and enzymatic analysis of MshA from *Corynebacterium glutamicum*: Substrate-assisted catalysis. *J. Biol. Chem.* **283**, 15834–15844
57. Teck, K. C., Bujnicki, J. M., Tan, T.-C., Huynh, F., Patel, B. K., and Sivaraman, J. (2008) The structure of sucrose phosphate synthase from *Halothermothrix orenii* reveals its mechanism of action and binding mode. *Plant Cell* **20**, 1059–1072
58. Wu, R., Asención Diez, M. D., Figueroa, C. M., Machtey, M., Iglesias, A. A., Ballicora, M. A., and Liu, D. (2015) The crystal structure of *Nitrosomonas europaea* sucrose synthase reveals critical conformational changes and insights into sucrose metabolism in prokaryotes. *J. Bacteriol.* **197**, 2734–2746
59. Batt, S. M., Jabeen, T., Mishra, A. K., Veerapen, N., Krumbach, K., Eggeling, L., Besra, G. S., and Fütterer, K. (2010) Acceptor substrate

discrimination in phosphatidyl-*myo*-inositol mannoside synthesis: Structural and mutational analysis of mannosyltransferase *Corynebacterium glutamicum* PimB′. *J. Biol. Chem.* **285**, 37741–37752
60. Fiebig, T., Cramer, J. T., Bethe, A., Baruch, P., Curth, U., Führing, J. I., Buettner, F. F. R., Vogel, U., Schubert, M., Fedorov, R., and Mühlenhoff, M. (2020) Structural and mechanistic basis of capsule *O*-acetylation in *Neisseria meningitidis* serogroup A. *Nat. Commun.* **11**, 4723
61. Bergfeld, A. K., Claus, H., Lorenzen, N. K., Spielmann, F., Vogel, U., and Mühlenhoff, M. (2009) The polysialic acid-specific *O*-acetyltransferase OatC from *Neisseria meningitidis* serogroup C evolved apart from other bacterial sialate *O*-acetyltransferases. *J. Biol. Chem.* **284**, 6–16
62. Rawat, A., Roy, M., Jyoti, A., Kaushik, S., Verma, K., and Srivastava, V. K. (2021) Cysteine proteases: Battling pathogenic parasitic protozoans with omnipresent enzymes. *Microbiol. Res.* **249**, 126784
63. Cheah, E., Austin, C., Ashley, G. W., and Ollis, D. (1993) Substrate-induced activation of dienelactone hydrolase: An enzyme with a naturally occurring Cys-His-Asp triad. *Protein Eng.* **6**, 575–583
64. Leščić Ašler, I., Štefanić, Z., Maršavelski, A., Vianello, R., and Kojić-Prodić, B. (2017) Catalytic dyad in the SGNH hydrolase superfamily: In-depth insight into structural parameters tuning the catalytic process of extracellular lipase from *Streptomyces rimosus*. *ACS Chem. Biol.* **12**, 1928–1936
65. Herrmann, K. W. (1962) Non-ionic-cationic micellar properties of dimethyldodecylamine oxide. *J. Phys. Chem.* **66**, 295–300
66. Strop, P., and Brunger, A. T. (2005) Refractive index-based determination of detergent concentration and its application to the study of membrane proteins. *Protein Sci.* **14**, 2207–2211
67. Low, K. E., and Howell, P. L. (2018) Gram-negative synthase-dependent exopolysaccharide biosynthetic machines. *Curr. Opin. Struct. Biol.* **53**, 32–44
68. Hoo, R., Lam, J. H., Huot, L., Pant, A., Li, R., Hot, D., and Alonso, S. (2014) Evidence for a role of the polysaccharide capsule transport proteins in pertussis pathogenesis. *PLoS One* **9**, e115243
69. Allen, A. G., Thomas, R. M., Cadisch, J. T., and Maskell, D. J. (1998) Molecular and functional analysis of the lipopolysaccharide biosynthesis locus *wlb* from *Bordetella pertussis*, *Bordetella parapertussis* and *Bordetella bronchiseptica*. *Mol. Microbiol.* **29**, 27–38
70. Hitchcock, P. J., and Brown, T. M. (1983) Morphological heterogeneity among *Salmonella* lipopolysaccharide chemotypes in silver-stained polyacrylamide gels. *J. Bacteriol.* **154**, 269–277
71. Wear, S. S., Hunt, B. A., Clarke, B. R., and Whitfield. (2020) Analysis of the topology and active-site residues of WbbF, a putative O-polysaccharide synthase from *Salmonella enterica* serovar Borreze. *J. Bacteriol.* **202**. e00625-19
72. Clarke, B. R., Cuthbertson, L., and Whitfield, C. (2004) Nonreducing terminal modifications determine the chain length of polymannose O antigens of *Escherichia coli* and couple chain termination to polymer export via an ATP-binding cassette transporter. *J. Biol. Chem.* **279**, 35709–35718
73. Larkin, M. A., Blackshields, G., Brown, N. P., Chenna, R., McGettigan, P. A., McWilliam, H., Valentin, F., Wallace, I. M., Wilm, A., Lopez, R., Thompson, J. D., Gibson, T. J., and Higgins, D. G. (2007) Clustal W and clustal X version 2.0. *Bioinformatics* **23**, 2947–2948
74. Robert, X., and Gouet, P. (2014) Deciphering key features in protein structures with the new ENDscript server. *Nucleic Acids Res.* **42**, W320–W324
75. Chang, A. C. Y., and Cohen, S. N. (1978) Construction and characterization of amplifiable multicopy DNA cloning vehicles derived from the P15A cryptic miniplasmid. *J. Bacteriol.* **134**, 1141–1156